Generation of two-color polarization-entangled photon pairs in a folded sandwich configuration

Masterarbeit

zur Erlangung des akademischen Grades
Master of Science
(M.Sc.)
im Fach Physik

eingereicht an der
Mathematisch-Naturwissenschaftlichen Fakultät
Institut für Physik
Humboldt-Universität zu Berlin

von
Herrn Chris Müller
geboren am 09.07.1989 in Königs Wusterhausen

Betreuung:

1. *Prof. Dr. Oliver Benson*
2. *Prof. Achim Peters, Ph.D.*

eingereicht am: *31. August 2015*

Abbreviations

APD	avalanche photo diode
cps	counts per second
BSM	Bell state measurement
DFG	difference frequency generation
FWHM	full width at half maximum
HWP	half-wave plate
SFG	sum frequency generation
SHG	second harmonic generation
SPDC	spontaneous parametric down-conversion
PPLN	periodically poled $LiNbO_3$
QM	quantum memory
QWP	quarter-wave plate
YVO_4	Yttrium orthovanadate

Abstract

Entanglement is a quantum mechanical phenomenon where two or more particles cannot be described with independent one particle states. This leads to counter-intuitive results because distant particles can influence each other instantaneously. This behavior can be exploited for different applications in quantum communications.

Entangled photons can be used to create entanglement between two distant quantum systems. This is needed in order to realize a quantum repeater, a necessity for long distance quantum communications. To establish entanglement between two dissimilar quantum systems, i.e. to create quantum hybrid systems, entangled photons with different wavelengths are needed, as well.

This thesis reports on a portable and tunable two-color entangled photon pair source. The entangled photons are created via spontaneous parametric down-conversion in a nonlinear crystal that is traversed twice. The setup is based on a purely geometrical principle for a broad tunability of the entangled photons. The experimental setup is used to generate polarization entangled photons at the Cs D1 line (894.3 nm) and the telecom O-band (1313.1 nm) as a proof of principle. After optimization of the setup, an entanglement fidelity of $75 \pm 2\%$ was obtained for these wavelengths.

Zusammenfassung

Verschränkung ist ein quantenmechanisches Phänomen, bei dem zwei oder mehr Teilchen nicht mehr unabhängig mit Einteilchen-Zuständen beschrieben werden können. Dies führt zu kontraintuitiven Ergebnissen, da weit entfernte Teilchen sich scheinbar instantan beeinflussen können. Exakt dieses Verhalten kann in verschiedensten Quantum-Kommunikationsanwendungen ausgenutzt werden.

Verschränkte Photonen können dazu verwendet werden, Verschränkung zwischen unterschiedlichen Quantensystemen herzustellen. Dies wird unter anderem benötigt, um einen Quantenrepeater zu realisieren, welcher für eine Quantenkommunikation über eine lange Distanz benötigt wird. Um Verschränkung zwischen zwei unterschiedlichen Quanten Systemen aufzubauen, z.B. zur Realisierung von Quanten Hybridsystemen, werden ebenfalls verschränkte Photonen mit unterschiedlichen Wellenlängen benötigt.

Diese Arbeit präsentiert eine transportable und spektral durchstimmbare polarisationsverschränkte Photonenpaar-Quelle mit Photonen unterschiedlicher Wellenlänge. Die verschränkten Photonenpaare werden durch parametrische Fluoreszenz in einem nichtlinearen Kristall erzeugt, welcher zweimal durchlaufen wird. Der Aufbau basiert auf einem geometrischen Prinzip, um eine hohe Durchstimmbarkeit der Wellenlängen zu erreichen. Der experimentelle Aufbau wird zur Verschränkung von Photonenpaaren bei der Cs D1 Linie (894.3 nm) und bei dem Telekom O-Band (1313.1 nm) benutzt. Nach einigen Optimierungen des Aufbaus wurde eine Verschränkungsreinheit von $75 \pm 2\%$ bei diesen Wellenlängen nachgewiesen.

Contents

1 Introduction

Secure communication became an important aspect of modern life with the appearance of the Internet and mobile electronic communication. Cryptography can be used to achieve safe communication [BKW13]. The idea is that the sender, Alice, uses a key to encrypt her message before she sends it to the receiver, Bob. He also has a key for decrypting the message. If an eavesdropper, Eve, tries to read the message, she can only obtain the encrypted message. The disadvantage of this method is that Alice and Bob have to share the key before they can communicate. However, they cannot use their communication channel for the key distribution because Eve could obtain the key from that unencrypted message.

One solution is that Alice and Bob use asymmetric keys [RSA78]. Alice receives a key from Bob to encrypt the message but the message cannot be decrypted with the same key. Since the message cannot be decrypted with that key, it can be shared publicly. For this reason that key is referred to as Bob's public key. Bob has a second key, his private key. With that he can decrypt the message from Alice. If Bob wants to send Alice a message, then he will use Alice's public key to encrypt the message and Alice will use her private key to decrypt the message.

The disadvantage of asymmetric encryption is, that its security is based on the assumption that solving certain number-theoretic problems is difficult [MOV96]. The result is that no public key scheme has been proven to be secure. While the algorithms for attacking an encrypted message are very time intensive, the time decreases with every improvement in computer technology. If quantum computers become a reality, asymmetric encryption would become unsafe since the quantum computer can solve these problems efficiently [NC10]. Quantum mechanics provides a solution for this problem: quantum communication [LSP98].

Bennett and Brassard showed in their BB84 protocol that it is possible to generate a key using quantum states [BB84]. The idea is to communicate with photons that have different polarizations. Alice generates a vertically, horizontally, diagonally or anti-diagonally polarized photon and sends it to Bob. He can decide to measure the vertical or diagonal polarization. If he measures in the vertical basis, then he obtains a defined result for a vertically or horizontally polarized photon but the result for a diagonally or anti-diagonally polarized photon will be random, and vice versa if he measures in the diagonal basis. Bob chooses the measured basis at random without knowing whether it is correct or not. Afterwards, Alice and Bob compare the bases they have chosen with each other on a classical communication channel and can generate a key from the photons where the basis were identical. This can be done by assigning each polarization a value of 0 or 1. With that, both obtain the same key over a long distance.

Eve can eavesdrop on the key generation process but the no-cloning theorem [WZ82] forbids copying a unknown quantum state. That means her measurement changes the polarization of the photon. She can emit a photon with same polarization as she measured but she does not know which basis is the correct basis and she has to chose one at random. Alice and Bob can check if Eve eavesdropped by

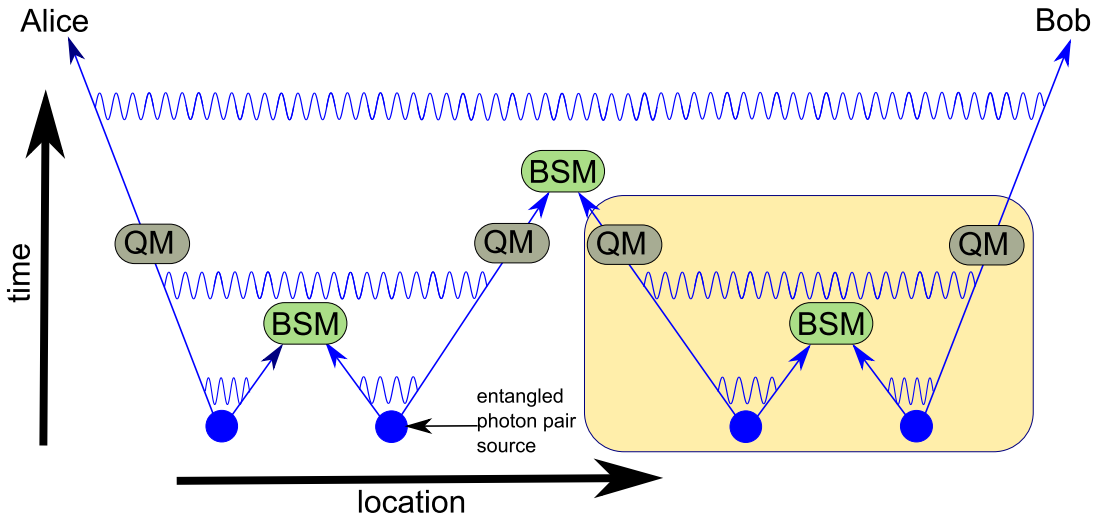

Figure 1: Quantum repeater schematic [BDC+98]. The quantum repeater (yellow box) needs at least two entangled photon pair sources. Entanglement is illustrated with wavy blue lines. Each photon source emits one entangled photon pair. The inner two photons of the quantum repeater undergo a Bell state measurement (BSM) and the other two are sent to different locations. A successful Bell state measurement leads to entanglement swapping, resulting in entanglement of the two outer photons. The quantum state is stored in quantum memories (QM) without destroying the entanglement. By repeating this procedure and storing several entangled pairs, the quality of the entanglement can even be improved (entanglement distillation). Cascading of identical repeater units will finally result in an entangled photon pair shared by Alice and Bob at arbitrary distance. In this way a long distance communication between Alice and Bob can be established.

comparing the results for some of the measurements made when both selected the same basis. If they have different results, they know that Eve eavesdropped and changed the state of the photons. In that case they will not use that key and stop their communication. Alice and Bob will not obtain the same result for every measurement because of errors from noise, but if the error is too high, then they know that there was likely an eavesdropper.

With the BB84 protocol a safe communication is possible, but fiber loses limit the optical communication range [SSR+11]. For instance, for a communication between Berlin and Munich (about 500 km) at a speed of 10 Gb/s this means that only 6280 bytes reach the receiver after one day. In classical communication that problem is solved by using a repeater, to refresh the signal after a certain distance. The no-cloning theorem forbids the renewal of the quantum state because it implies that the state is known.

The corollary of this is that long distance communication with quantum states seems impossible. However, the problem with the no-cloning theorem can be overcome by using a quantum repeater that relies on entangled photons [BDC+98]. Figure 1 shows the basis of a quantum repeater where Alice and Bob share one entangled photon pair. The quantum repeater uses several entangled photon pairs instead of one photon for the communication. By storing several entangled photon pairs in quantum memories without destroying the entanglement, it is even possible to improve the quality of the entanglement (entanglement distillation).

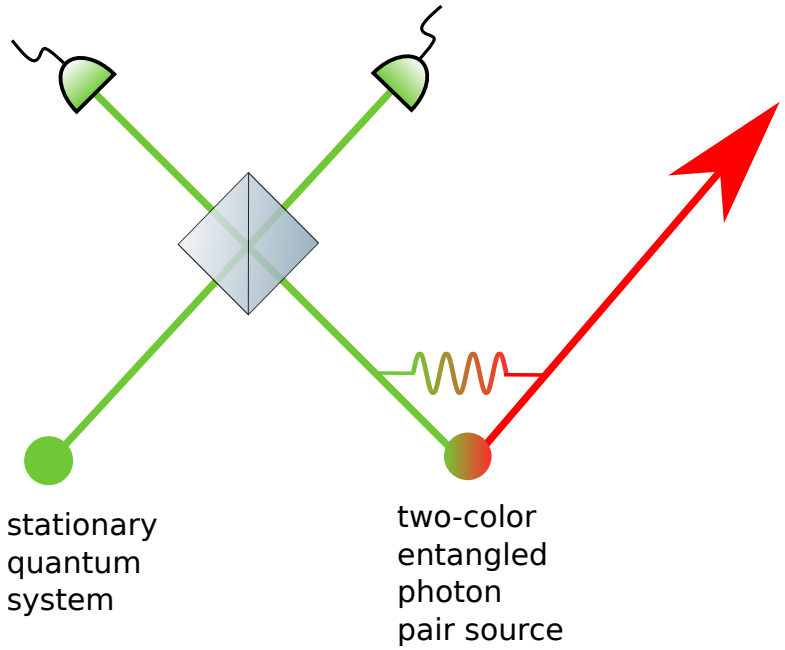

Figure 2: Quantum state swapping as interface. One photon from a two-color entangled photon pair source and a photon from another (stationary) quantum system interfere at a beam splitter. The photon coming from the left is assumed to be entangled with an internal (stationary) state of the quantum system. A Bell measurement performed with the help of the beam splitter can swap the quantum state, i.e., after the measurement the quantum system is entangled with the telecom photon on the right.

Many quantum systems work on different wavelengths and two quantum systems with different wavelengths cannot communicate with each other. The quantum memory of the quantum repeater could be realized by using electrons [GYS+06] or holes [BGD+09] in quantum dots. A wavelength in the telecom band should be used for an effective quantum repeater, but a quantum memory would be difficult to realize at a telecom wavelength. A solution is to use an interface between the quantum system and the telecom band. The interface can be an entangled photon pair source where the pair consists of two photons with different wavelengths. Then, an entangled state between a stationary quantum system and, for example, a shorter wavelength photon can be swapped to a telecom photon (Figure 2). Thus needed for various application in quantum information processing. Possible sources are atoms [VWS+06], ions [BMD+04], semiconductor quantum dots [GFT+12], color defect centers [TCT+10], and super conducting qubits [WSB+04].

One of the brightest entangled photon pair sources relies on spontaneous parametric down-conversion (SPDC) in a nonlinear crystal [KMW+95]. A two-color source with different photon wavelengths can be realized by adjusting the phase matching of this nonlinear crystal [PML+04; HHP+09; SSB+13]. The collinear alignments i.e. crystal Sagnac source [HHP+09], crossed crystal [TW08] and the folded sandwich configuration [SRJ+13], enable further integration into other systems. An example is a quantum hybrid system that consists of two different quantum systems in a joint quantum state.

In this work a tunable two-color entangled photon pair source in a modified folded sandwich configuration for quantum repeater and quantum interface applications is set up. The two target wavelengths are 894.3 nm an 1313.1 nm, which correspond to the cesium D1 line [Ste08] and a wavelength in the telecom O band [Pas08]. The Cs D1 line was chosen as an atomic transition standard. More importantly, it is near typical wavelengths of the excitonic transition in InGaAs quantum dots [DSP+10]. This source could also be used for quantum hybrid architectures involving atoms, molecules or quantum dots to transfer their information into a fiber.

The source relies on spontaneous parametric down-conversion in a nonlinear crystal to create the entanglement. For this reason, Section 2 gives an introduction to nonlinear processes, followed by the basics of entanglement and a discussion of different entangled photon pair source configurations. The setup of the modified folded sandwich configuration is explained in detail in Section 3. The experimental results such as the tunability and the entanglement measurements of the setup are presented in Section 4.

2 Principles

This chapter deals with the theoretical background needed to set up an entangled photon pair source based on a nonlinear crystal. Section 2.1 discusses the basics of nonlinear optics to clarify the working of the nonlinear crystal. A short introduction to entanglement is given in Section 2.2. Finally, two entangled photon pair source configurations are introduced in Section 2.3.

2.1 Nonlinear optics

Nonlinear optics describes the interaction between light and matter for high intensity incident light fields. More precisely, it deals with the nonlinear relation of the polarization $P(t)$ (dipole moment per unit volume) and an applied optical electric field $E(t)$ [Boy13].

The polarization $P(t)$ induced by a low intensity electric field $E(t)$ can be approximated by the linear relation

$$P(t) = \epsilon_0 \chi^{(1)} E(t) \tag{2.1}$$

where ϵ_0 is the permittivity of free space and $\chi^{(1)}$ is the linear susceptibility. Higher orders of $P(t)$ become significant if the applied field is large. A more general expression of Equation (2.1) is

$$P(t) = \epsilon_0 \left(\chi^{(1)} E(t) + \chi^{(2)} E^2(t) + \chi^{(3)} E^3(t) + ... \right) \tag{2.2}$$

where $\chi^{(n)}$ is a (n+1)-rank tensor. By using Equation (2.2) for the polarization it is possible to describe many nonlinear effects, such as frequency mixing, the piezoelectric effect, and Pockels effect.

The second-order term of Equation (2.2)

$$P^{(2)}(t) = \epsilon_0 \chi^{(2)} E^2(t) \tag{2.3}$$

is relevant for this work since it is the first higher order term, which allows for the generation of new frequencies. The second-order susceptibility $\chi^{(2)}$ is a third-rank tensor. It becomes zero if the material has inversion symmetry, which is the case for liquids, gases and many crystals. The consequence is that the second-order polarization occurs only if the material lacks inversion symmetry. In the following it is assumed that any discussed nonlinear material has no inversion symmetry.

If the incident field $E(t)$ is assumed to be a superposition of two monochromatic waves

$$E(t) = E_1 e^{-i\omega_1 t} + E_2 e^{-i\omega_2 t} + c.c., \tag{2.4}$$

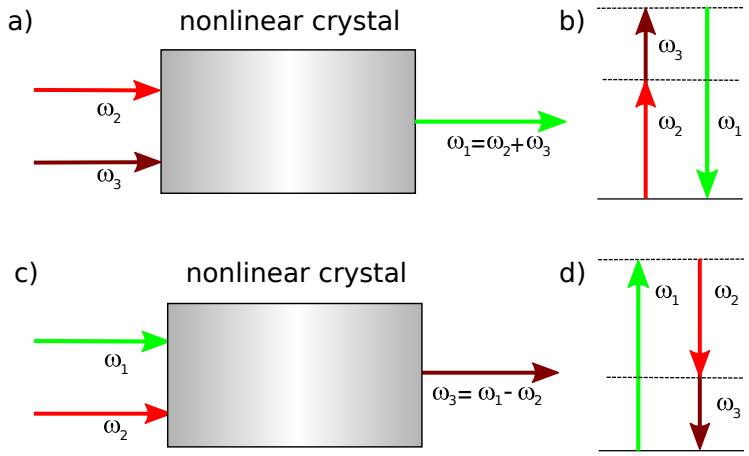

Figure 3: Geometric interaction and energy levels for SFG and DFG. In SFG a) the frequency of the generated field is the sum of the applied fields. In terms of a photon energy level diagram b) this means that two photons with the frequency ω_2 and ω_3 are destroyed and a photon with the frequency ω_1 is created simultaneously in this process. The energy level shows that the energy of the two destroyed photons is equal to the energy of the generated photon. Note that the energy levels are not the energy eigenlevels of the atom but rather show the energy of the photons. SHG is quite similar to the SFG, but the two destroyed photons have the same energy ($\omega_2 = \omega_3$). This means that the created photon has exactly twice the energy of an incident photon. For DFG c) the frequency of the generated wave is the difference of the applied fields. The energy conservation in the energy level d) shows that for every created photon with the frequency ω_3 a photon with the higher input frequency ω_1 is destroyed and the photon with the lower input frequency ω_2 is created. Therefore the lower input field with the frequency ω_2 is amplified in this process.

then the second-order nonlinear polarization has the form

$$P^2(t) = \epsilon_0 \chi^2 \left[\underbrace{E_1^2 e^{-2i\omega_1 t}}_{SHG} + \underbrace{E_2^2 e^{-2i\omega_2 t}}_{SHG} + \underbrace{2E_1 E_2 e^{-i(\omega_1+\omega_2)t}}_{SFG} + \underbrace{2E_1 E_2^* e^{-i(\omega_1-\omega_2)}}_{DFG} + c.c. + 2\epsilon_0 \left(\underbrace{E_1 E_1^* + E_2 E_2^*}_{const.} \right) \right]. \tag{2.5}$$

Besides the constant terms, this equation describes the second harmonic generation (SHG), sum frequency generation (SFG), and difference frequency generation (DFG). Figure 3 gives a short explanation of these three generation types.

For all these generation processes the requirements of both conservation of energy

$$\omega_1 = \omega_2 + \omega_3 \tag{2.6}$$

and conservation of momentum

$$k_1 = k_2 + k_3 \tag{2.7}$$

must to be fulfilled. The conservation of momentum is referred to as phase matching.

It is very difficult to fulfill the phase matching condition for different frequencies. For this reason Section 2.1.1 discusses the phase matching in a nonlinear material.

This work uses a special case of DFG, the spontaneous parametric down-conversion, which is explained in Section 2.1.2. The bandwidth of the generated photons in a nonlinear process is a specific property of the setup. Section 2.1.3 gives a short introduction over the different broadening effects and estimates the bandwidth of photons generated in a nonlinear crystal.

2.1.1 Phase matching

The behavior of materials with nonlinear optical properties can be understood by considering the material as a large collection of oscillating dipoles (atoms). A dipole radiates an electric field when it oscillates. The phase of this oscillation depends on the phase of the incident light. If there is more than one oscillating dipole and the relative phase of these oscillations is in phase, then the radiated field will add constructively. Since the material has a massive number of such oscillating dipoles, the result is that the oscillating dipoles can amplify the intensity of an incident frequency, provided that the incident light fields have the correct phase and energy. However, the involved fields must fulfill the condition known as phase matching that was given in Equation (2.7).

The efficiency of the nonlinear process is quite low and decreases with increasing mismatch. The phase mismatch for DFG is given by

$$\Delta k = k_1 - k_2 - k_3 \tag{2.8}$$

where k_1, k_2 and k_3 are the wave vectors of the incident and generated light. The highest intensity electric field is generated in the special case where $\Delta k = 0$. The phase mismatch dependent efficiency of a three wave mixing process can be described with [MW95]

$$\eta(\Delta k) \sim \frac{\sin^2(\Delta k L/2)}{(\Delta k L/2)^2} = \mathrm{sinc}^2(\Delta k L/2). \tag{2.9}$$

The generated fields are out of phase after a distance

$$L_{coh} = \frac{2}{\Delta k}, \tag{2.10}$$

called interaction length which decreases with increasing phase mismatch Δk. Since the generated fields are out of phase after the interaction length, the energy of the generated fields can then be transferred to the incident fields, which lowers the efficiency. It is very difficult to achieve $\Delta k = 0$ because of the wavelength dependent refractive index of the material.

One approach to fulfilling the phase matching condition is to use a birefringent material [Boy13]. The refractive index of a birefringent material depends on the polarization of the light field. There are two common tuning techniques used to reduce the phase mismatch: angle tuning and temperature tuning. Angle tuning utilizes the polarization dependence of the refractive index. Tilting the crystal with respect to its optical axis results in a change in the refractive indices for the

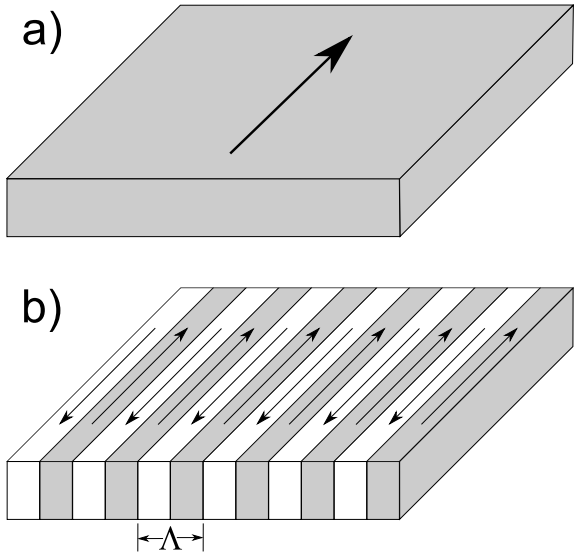

Figure 4: Comparison between a uniaxial and a period poled crystal. A a) uniaxial crystal has exactly one orientation of its optical axis. In contrast, b) the optical axis orientation of a periodic poled crystal alternates with the periodicity Λ. This results in a higher efficiency for nonlinear processes.

different wavelengths. Temperature tuning uses the fact that most optical properties are temperature dependent and that $\frac{\Delta n}{\Delta T}$ also differs for different wavelengths. By changing the temperature of a nonlinear crystal it is possible to minimize the phase mismatch for a more efficient three wave mixing process.

There are some situations where a birefringent material cannot be used, or the birefringence in the wavelength range of interest is too small to compensate the dispersion. In such cases, a periodically poled crystal is used in a technique known as quasi-phase matching. A uniaxial single crystal has exactly one optical axis (Figure 4a). The concept behind quasi-phase matching is the use of a periodic poled crystal where the optical axis changes as shown in Figure 4b. The periodicity Λ with which the optical axis changes is chosen in such way that the optical axis changes its orientation when the generated field starts to transfer energy back to the fundamental field. The result of the change in optical axis is that the amplitude of the generated field continues to increase.

If there is no phase mismatch, then the field amplitude in a nonlinear crystal with a single optical axis increases linearly with the propagation length as shown in Figure 5 (blue line). If there is a phase mismatch, then the field amplitude varies periodically with the propagation distance (see Figure 5 green line). If a periodic poled crystal is used, then the period Λ of the optical axis is twice as long as the coherent length L_{coh} in the ideal case. That means that the generated wave can efficiently collect energy because the orientation of the optical axis changes when the amplitude starts to decrease. The behavior of the quasi-phase matching is shown in Figure 5 (red line). With quasi-phase matching, it is possible to obtain a phase

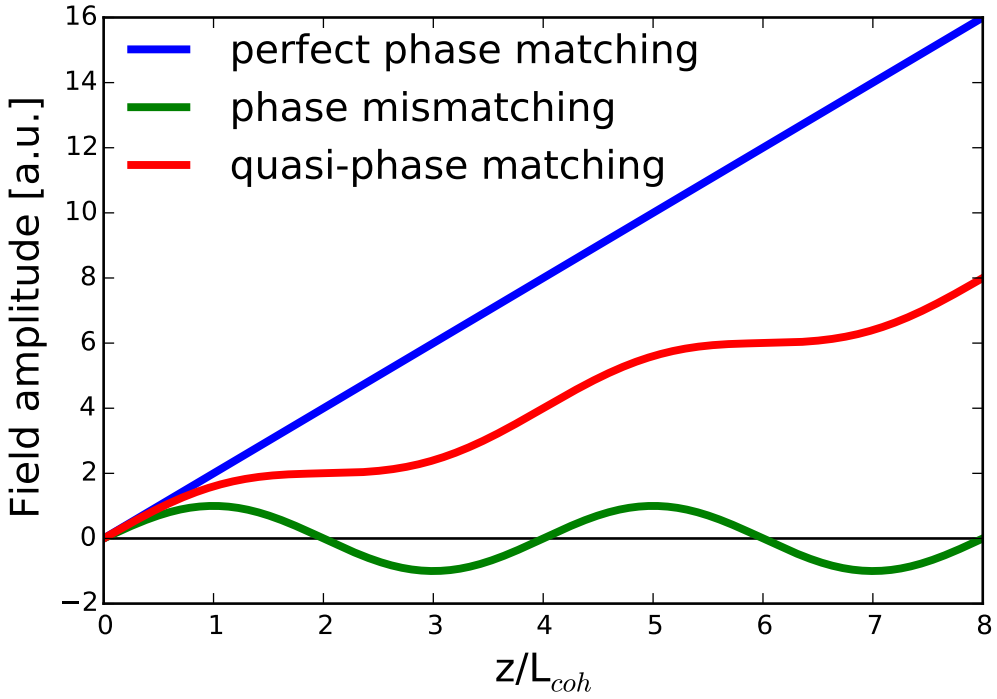

Figure 5: Comparison of different phase matching conditions. The blue line shows the case of optimal phase matching, where the field amplitude of the generated field is increasing linearly with the length of the nonlinear material. If there is a phase mismatch (green line), then the generated field amplitude oscillates because it transfers energy back to the fundamental fields. The generated field amplitude also oscillates in the case of quasi-phase matching (red line), but increases linearly with the material length as well.

mismatch for the first-order of

$$\Delta k_{QPM} = k_1 - k_2 - k_3 - \frac{2\pi}{\Lambda}, \tag{2.11}$$

which is more flexible then the phase matching condition of Equation (2.8), because Λ can be changed easily. The result is a higher efficiency for the nonlinear process.

The quasi-phase matching can be achieved for example by periodically applying a voltage to a nonlinear material [YNS+93] or by periodic changing of the parameters during the growing process of the crystal [FMH+80].

2.1.2 Spontaneous parametric down-conversion

Spontaneous parametric down-conversion (SPDC) is a special case of DFG, in which there is only one incident field with the frequency ω_p. This incident field is referred as the pump light. In the photon picture SPDC can be explained as follows: A photon interacts with the nonlinear material and is split in two photons with the frequencies ω_s and ω_i (Figure 6) [BEZ13]. For historical reasons, the higher frequency photon ω_s is called signal photon and with the lower frequency photon ω_i is called idler photon.

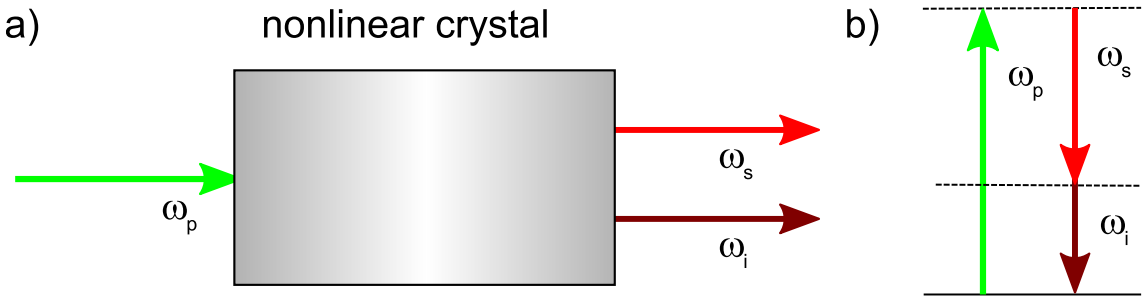

Figure 6: a) Geometry and b) level scheme picture of SPDC. The pump photon ω_p interacts with the nonlinear material and creates the signal ω_s and idler ω_i photons. A periodic poled crystal (see Section 2.1.1) is often used as a nonlinear material to achieve a higher SPDC efficiency.

There are different types of the SPDC processes, which are defined by the photon polarizations [ASJ+13]. In type-I down-conversion the pump photon is orthogonally polarized to the signal and idler photons, which have the same polarization. In type-II down-conversion signal and idler photons are polarized orthogonal to each other and one of the generated photons has the same polarization as the pump photon. Finally, in type-0 down-conversion all photons have the same polarization. Table 1 shows the different possibilities for these three processes in a uniaxial crystal.

It will be shown later that spontaneous parametric down-conversion can be used to create an entangled photon pair source.

Table 1: Different phase matching processes in a uniaxial crystal. The refractive index of the extraordinary (e) axis is higher than that of the ordinary axis (o) in a positive uniaxial crystal. As a consequence, an ordinary photon is needed as a pump photon to fulfill the phase matching condition. The ordinary pump photon can split up into two extraordinary photons (type-I), one ordinary and one extraordinary photon (type-II) or in two ordinary photons (type-0). The situation for the negative uniaxial crystal is exactly vice versa.

	positive uniaxial ($n_e > n_o$)	negative uniaxial ($n_e < n_o$)
Type-I	o→e+e	e→o+o
Type-II	o→o+e	e→e+o
Type-0	o→o+o	e→e+e

2.1.3 Bandwidth of photons created in a nonlinear crystal

The photons generated in a nonlinear crystal have a bandwidth determined by the phase matching condition and energy conservation [Tan96]. The main influences are the linewidth of the pump laser, the angular divergence of the pump wave and the crystal properties.

Different angles between the optical axis and the propagation direction lead to different refractive indices in a birefringent crystal. This leads to a range of Δk_p for a finite beam divergence $\Delta\Theta_p$ of the pump light, yielding a range of values for the sum of the idler and signal propagation vectors $\Delta(k_s + k_i)$. This effect is significant

when the pump light propagates along a non-principal axis of the nonlinear material. In the direction of a principal axis this effect is negligible compared to other causes of broadening. Propagating along the principal axis is called 'non-critical' phase matching because the generated wavelength is insensitive to slight variations in the propagation direction of the pump beam. For further discussion it can be assumed that the pump beam propagates along a principal axis. Then the dominant bandwidth broadening mechanism is due to the finite interaction length of the crystal.

A Taylor expansion of Equation (2.8) with respect to the signal frequency ω_s leads to

$$\Delta k(\omega_s + \Delta\omega_s) = \Delta k_0 + \frac{\partial \Delta k}{\partial \omega_s}\Delta\omega_s + ... \tag{2.12}$$

where Δk_0 is the constant phase mismatch [Pow11]. Here the variation from the phase matched point $\Delta k_0 = 0$ is of interest, yielding

$$\Delta k(\omega_s + \Delta\omega_s) = \frac{\partial \Delta k}{\partial \omega_s}\Delta\omega_s + ... \tag{2.13}$$

The bandwidth of the photons generated in a nonlinear crystal can be expressed as the change of the frequency before the efficiency is below a certain threshold. Equation (2.9) gives the efficiency of a three wave mixing process with phase mismatch by $\mathrm{sinc}^2(\Delta kL/2)$, where the phase mismatch Δk depends on the variation of the frequency $\Delta\omega_s$. The threshold probability can be chosen differently depending on the specific case [Pow11; She03]. In this work the definition of the full width at half maximum (FWHM) [Pow11] is used so that the efficiency holds

$$\mathrm{sinc}^2(\Delta kL/2) \geq 0.5 \tag{2.14}$$

hence

$$\frac{0.886\pi}{2} \quad \geq \quad \left|\frac{\Delta kL}{2}\right|, \tag{2.15}$$

which ensures that the efficiency of the nonlinear process is at least 50 % of the maximum possible. Combining Equations (2.13) and (2.15) leads to a bandwidth of

$$\Delta\omega_s = \pm\frac{0.886\pi}{L\left|\frac{\partial \Delta k}{\partial \omega_s}\right|} \tag{2.16}$$

or for the full width to

$$\Delta\omega_{s_{FWHM}} = 2\frac{0.886\pi}{L\left|\frac{\partial\Delta k}{\partial\omega_s}\right|}. \tag{2.17}$$

It can be seen that a longer crystal length L leads to a narrower bandwidth of the generated photons. The partial derivative

$$\frac{\partial\Delta k}{\partial\omega_s} = \frac{\partial}{\partial\omega_s}\left(k_p - k_s - k_i\right) \tag{2.18}$$

will be simplified in the following.

The pump frequency ω_p is independent from the variation of ω_s, with the result that the wave vector k_p is also independent of ω_s

$$\frac{\partial k_p}{\partial\omega_s} = 0. \tag{2.19}$$

The derivative of the idler wave vector depends on the frequency variation, with the relation

$$\frac{\partial k_i}{\partial\omega_s} = \frac{\partial k_i}{\partial\omega_i}\frac{\partial\omega_i}{\partial\omega_s} = -\frac{\partial k_i}{\partial\omega_i} \tag{2.20}$$

since $\omega_i = \omega_p - \omega_s$. With these results it is possible to simplify Equation (2.18) to

$$\frac{\partial\Delta k}{\partial\omega_s} = -\frac{\partial k_s}{\partial\omega_s} + \frac{\partial k_i}{\partial\omega_i}. \tag{2.21}$$

Combining Equation (2.21) with the definition of the wave vector $k = n\omega/c$ and putting the result into Equation (2.17) leads to

$$\Delta\omega_s = 2\frac{0.886\pi c}{L\left|n_s - n_i + \omega_s\left(\frac{\partial n_s}{\partial\omega_s}\right) - \omega_i\left(\frac{\partial n_i}{\partial\omega_i}\right)\right|} \tag{2.22}$$

where L is the interaction length, and n_s and n_i the refractive indices for the signal and idler photons.

The refractive index of a material is often given by the Sellmeier equation, which is wavelength dependent. It is possible to rewrite the Sellmeier equation for one material as a frequency dependent equation, but it is more useful to reformulate Equation (2.22). The wavelength λ can be expressed as

$$\lambda = \frac{c}{f} \tag{2.23}$$

$$= \frac{2\pi c}{\omega} \tag{2.24}$$

yielding for the derivative

$$\frac{\partial n}{\partial \omega} = \frac{\partial n}{\partial \lambda}\frac{\partial \lambda}{\partial \omega} \tag{2.25}$$

$$\rightarrow \frac{\partial n}{\partial \omega} = -\frac{2\pi c}{\omega^2}\frac{\partial n}{\partial \lambda}. \tag{2.26}$$

The bandwidth of the photons from Equation (2.22) can be reformulated with Equation (2.26) as

$$\Delta\omega_s = 2\frac{0.886\pi c}{L\left|n_s - n_i - \lambda_s\left(\frac{\partial n_s}{\partial \lambda_s}\right) + \lambda_i\left(\frac{\partial n_i}{\partial \lambda_i}\right)\right|} \tag{2.27}$$

to obtain a wavelength dependent expression for the bandwidth of the generated photons.

As an example, the bandwidth of the photons generated in a 40 mm long lithium niobate crystal doped with 5 % magnesium oxide will be discussed. The wavelength dependent refractive index and its derivative are given in Appendix A.2. The pump wavelength is chosen to be 532 nm, the signal wavelength 894.3 nm and the idler wavelength 1313.1 nm. The photons generated in the extraordinary axis of such a configuration have a bandwidth of $\Delta\omega_s \approx 861$ GHz.

A relation between the bandwidth in hertz and meters can be derived from Equation (2.24)

$$\Delta\lambda = \frac{2\pi c}{\omega^2}\Delta\omega, \tag{2.28}$$

which yields a bandwidth of $\Delta\lambda_s \approx 0.37$ nm for the signal photons in the lithium niobate crystal.

Moreover, the energy conservation from Equation (2.6) gives a relation for the different bandwidths

$$\Delta\omega_p = \Delta\omega_s + \Delta\omega_i \tag{2.29}$$

and shows that any bandwidth of the pump beam $\Delta\omega_p$ leads to bandwidth for the signal photons $\Delta\omega_s$. However, the bandwidth of a continuous wave laser as used in this work can be assumed as $\Delta\omega_p \approx 0$, with the result that signal and idler photons have the same bandwidth $|\Delta\omega_s| = |\Delta\omega_i|$.

In conclusion, there are different mechanisms which broaden the spectral bandwidth of the generated photon pairs. The crystal and the laser determine which broadening mechanism is the significant one.

2.2 Entanglement

Quantum mechanics is a fundamental theory in physics which can explain many different phenomena on the nanoscopic scale. Several results of quantum mechanics are unexpected and difficult to imagine. Entanglement is one of these strange occurrences. This section discusses the basis of entanglement and explains the measurements needed to verify entanglement in a setup.

2.2.1 Fundamentals

Entanglement is a quantum mechanical phenomenon in which a system of two or more particles can only described as one inseparable state [BEZ13]. The consequence is that a measurement of one particle can determine the state of the whole quantum system.

If an entangled photon pair source emits vertically or horizontally polarized photon pairs in which both photons of one pair have the same polarization, then the system can be described quantum mechanically as

$$|\Psi\rangle = \frac{1}{\sqrt{2}} \left(|VV\rangle + e^{i\phi} |HH\rangle \right) \tag{2.30}$$

where the phase ϕ is determined by the source. For simplicity it is assumed that ϕ=0. Equation (2.30) shows an entangled state with the interesting characteristic that neither photon has a defined polarization. A measurement of a photon gives a completely random result for the vertical or horizontal polarization. If the polarization of one photon is measured, then the polarization of the other photon is defined immediately as well. The entangled state persists even if the photons are separated before the measurement. This leads to a non-locality because the photons can be separated by a long distance during the measurement of one of these photons.

Entanglement is quantum mechanically a superposition between different product states [NC10]. The maximally entangled two particle states are called the Bell states. The Bell states for two polarized entangled photons are

$$|\Psi^+\rangle = \frac{1}{\sqrt{2}} \left(|HV\rangle + |VH\rangle \right) \tag{2.31}$$

$$|\Psi^-\rangle = \frac{1}{\sqrt{2}} \left(|HV\rangle - |VH\rangle \right) \tag{2.32}$$

$$|\Phi^+\rangle = \frac{1}{\sqrt{2}} \left(|VV\rangle + |HH\rangle \right) \tag{2.33}$$

$$|\Phi^-\rangle = \frac{1}{\sqrt{2}} \left(|HH\rangle - |VV\rangle \right). \tag{2.34}$$

Note that these four equations form an orthonormal base. That means that they can be distinguished by a suitable quantum measurement.

An appropriate method to measure polarized entangled photon pairs will be discussed in the next section.

2.2.2 Entanglement measurement

It is difficult to construct a source which emits highly entangled photons. That is why it is very important to quantify the entanglement of a source.

One possibility to verify the entanglement of two photons is to measure the Bell state fidelity [WGP+07]. The fidelity is the overlap between the wave function of photons and the Bell state (see Section 2.2.1). The fidelity for the Bell state $|\Phi^+\rangle$ (see Equation (2.33)) is defined as

$$F_{\Phi^+} = \langle\Phi^+|\,\rho\,|\Phi^+\rangle \tag{2.35}$$

where ρ is the density matrix of the measured state. The state is entangled if $F_{\Phi^+} > 1/2$ [TH00]. The density matrix can be written as

$$\rho = \sum_{i,j=1}^{4} \rho_{ij}\,|u_i\rangle\,\langle u_j| \tag{2.36}$$

where the probability P_i to find a photon in the state i is given by the coefficient ρ_{ii} [Die15]

$$P_i = \rho_{ii} = \langle u_i|\,\rho\,|u_i\rangle\,. \tag{2.37}$$

A coincidence measurement of the two orthogonal polarization states i and j leads to the probability P_i

$$P_i = \frac{N_{ii}}{N_{ii} + N_{ij} + N_{ji} + N_{jj}}. \tag{2.38}$$

Vertical and horizontal polarization can be chosen as the two orthogonal polarization states, which leads to

$$|u_1\rangle = |HH\rangle \tag{2.39}$$
$$|u_2\rangle = |HV\rangle \tag{2.40}$$
$$|u_3\rangle = |VH\rangle \tag{2.41}$$
$$|u_4\rangle = |VV\rangle\,. \tag{2.42}$$

This choice of the basis yields

$$\langle u_1|\Phi^+\rangle = \frac{1}{\sqrt{2}} \qquad \langle u_2|\Phi^+\rangle = 0 \qquad \langle u_3|\Phi^+\rangle = 0 \qquad \langle u_4|\Phi^+\rangle = \frac{1}{\sqrt{2}}. \tag{2.43}$$

With that the fidelity can be formulated as

$$F_{\Phi^+} = \langle\Phi^+| \sum_{i,j=1}^{4} \rho_{ij} |u_i\rangle \langle u_j|\Phi^+\rangle \tag{2.44}$$

$$= \sum_{i,j=1}^{4} \rho_{ij} \langle\Phi^+|u_i\rangle \langle u_j|\Phi^+\rangle \tag{2.45}$$

$$= \frac{1}{2}(\rho_{11} + \rho_{14} + \rho_{41} + \rho_{44}) \tag{2.46}$$

$$= \frac{1}{2}(P_H + \rho_{14} + \rho_{41} + P_V) \tag{2.47}$$

with the chosen basis the probability ρ_{11} corresponds to the probability P_H and ρ_{44} corresponds to the probability P_V. The probabilities ρ_{14} and ρ_{41} cannot be expressed in the HV basis. Therefore additional polarization bases must be introduced

$$|D\rangle = \frac{|H\rangle + |V\rangle}{\sqrt{2}} \tag{2.48}$$

$$|A\rangle = \frac{|H\rangle - |V\rangle}{\sqrt{2}} \tag{2.49}$$

$$|R\rangle = \frac{|H\rangle + i\,|V\rangle}{\sqrt{2}} \tag{2.50}$$

$$|L\rangle = \frac{|H\rangle - i\,|V\rangle}{\sqrt{2}} \tag{2.51}$$

where a two particle state can be written as

$$|D\rangle\,|D\rangle = |DD\rangle = \frac{1}{2}(|HH\rangle + |VH\rangle + |HV\rangle + |VV\rangle) \tag{2.52}$$

$$= \frac{1}{2}(|u_1\rangle + |u_2\rangle + |u_3\rangle + |u_4\rangle) \tag{2.53}$$

The other two particle states can be expressed analogously.

The probability in the diagonal basis is

$$P_D = \langle DD|\rho|DD\rangle = \frac{1}{4}\sum_{i,j}^{4} = \rho_{ij} \tag{2.54}$$

and can be calculated analogously for the other bases. Using a combination of the diagonal and anti-diagonal basis yields

$$P_D + P_A = \langle DD|\rho|DD\rangle + \langle AA|\rho|AA\rangle \tag{2.55}$$

$$= \frac{1}{2}(\rho_{11} + \rho_{41} + \rho_{22} + \rho_{23} + \rho_{32} + \rho_{33} + \rho_{41} + \rho_{44}) \tag{2.56}$$

$$= \frac{1}{2}(1 + \rho_{14} + \rho_{41} + \rho_{23} + \rho_{23}). \tag{2.57}$$

In the last step the property of the density matrix $\mathrm{Tr}(\rho)=\rho_{11}+\rho_{22}+\rho_{33}+\rho_{44}=1$ is used. Similar results can be obtained for the last bases

$$P_R + P_L = \frac{1}{2}(1 - \rho_{14} - \rho_{41} + \rho_{32} + \rho_{32}). \tag{2.58}$$

According to that the probabilities ρ_{14} and ρ_{41} can be written as a combination of the Equations (2.57) and (2.58)

$$\rho_{14} + \rho_{41} = P_D + P_A - (P_R + P_L), \tag{2.59}$$

which leads for the Bell state fidelity of Equation (2.47) to

$$F_{\Phi^+} = \frac{1}{2}\left(P_H + P_V - (P_R + P_L) + P_H + P_V\right). \tag{2.60}$$

The result is that the fidelity can be determined if the probabilities for the three polarization bases are known. The probabilities can be obtained by measuring in different polarization bases (ij=H/V,D/A,R/L)

$$V_{ij} = \frac{N_{ii} + N_{jj} - (N_{ij} + N_{ji})}{N_{ii} + N_{jj} + N_{ij} + N_{ji}} \tag{2.61}$$

where N_{ij} are the coincidence count rates for the different polarizations. A coincidence count means that photon 1 is detected in state i, while photon 2 is detected in state j. The definition from Equation (2.61) can be rewritten as

$$V_{ij} + 1 = \frac{2(N_{ii} + N_{jj})}{N_{ii} + N_{jj} + N_{ij} + N_{ji}}. \tag{2.62}$$

Combining this definition and Equation (2.60) leads to

$$F_{\Phi^+} = \frac{1}{4}\left(1 + V_{HV} + V_{DA} - V_{LR}\right), \tag{2.63}$$

which shows that it is necessary to measure the coincidence counts in different polarization bases to obtain the fidelity of a system. It is possible to project the polarization into V/H or D/A base with a polarization filter [JKM+01]. To measure in R/L basis an additional quarter-wave plate (QWP) is needed. Table 2 shows some examples of projecting into different polarization bases with the two different polarization filters A and B of the experimental setup shown in Figure 7. With that setup it is possible to obtain the fidelity of an entangled photon pair source.

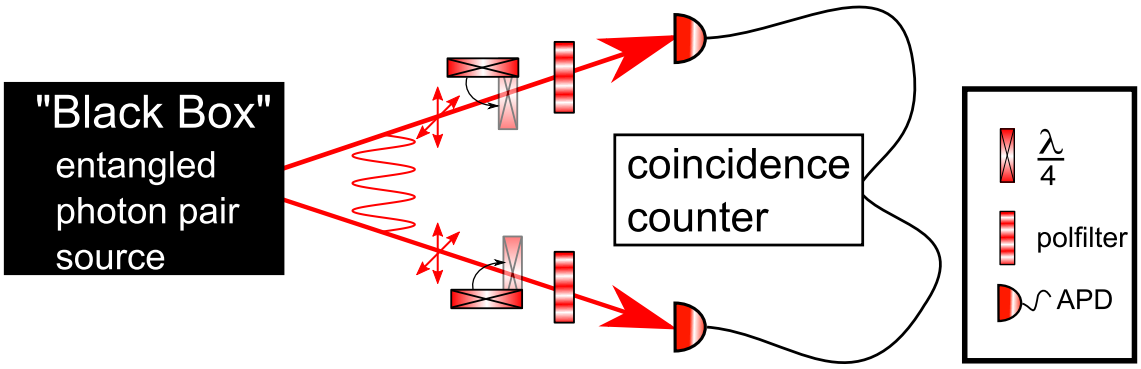

Figure 7: Coincidence measurement for an entangled photon pair source. The photon pair is separated spatially in two different arms. Each arm has a polarization filter and a quarter-wave plate. Combining these makes it possible to measure in different polarization bases (see Table 2). With the detector in each arm it is possible to measure the coincidence counts of both arms.

Table 2: Projection into different polarization bases. A combination of two polarization filters A and B together with two quarter-wave plates is necessary for measurements in different polarization bases. The quarter-wave plates are only needed to measure in circular bases.

	arm 1		arm 2	
basis	Θ_A	Θ_{QWP}	Θ_B	Θ_{QWP}
VV	0°	-	0°	-
HV	90°	-	0°	-
DV	45°	-	0°	-
AV	-45°	-	0°	-
RR	0°	-45°	0°	-45°
LL	0°	45°	0°	45°

2.3 Previous entangled photon pair creation schemes

There are different entangled photon pair sources that use a down-conversion process [HHP+09; TW08; SRJ+13]. Section 2.3.1 deals with the crossed crystal configuration, which uses two nonlinear crystals [TW08]. In contrast, the folded sandwich configuration described in Section 2.3.2 uses only one nonlinear crystal [SRJ+13]. Both setups need a compensation crystal after the generation scheme due to the dispersion in the setups. The need for such a compensation crystal will be discussed in detail in Section 3.2.

2.3.1 Crossed crystals

The crossed crystal configuration uses two identical nonlinear crystals to generate entangled photon pairs via SPDC [TW08]. The optical axis of the first crystal is orthogonal to the optical axis of the second crystal (see Figure 8).

For a type-0 SPDC process the diagonally polarized pump light can generate vertically polarized photon pairs in the first crystal. Since the optical axis of the second crystal is rotated by 90°, the pump light can generate horizontally polarized photon pairs in the second crystal. The focal point of the pump light is between the crystals to achieve a symmetric configuration. For simplicity it is assumed in Figure 8 that the SPDC occurs in the middle of each crystal.

The probability for generating more than one pair by passing through this configuration is low because of the chosen intensity of the pump light. The result is that one vertically *or* horizontally polarized photon pair can be found after the second crystal. The photon pairs in this setup are polarization-entangled if they are indistinguishable except for the polarization.

The disadvantage is of using two nonlinear crystals is that slight differences in defects or temperature between the crystals can lead to a different quasi-phase matching condition. The result is that, the photon pairs are distinguishable spectrally, and thus the polarization-entanglement is diminished, or even completely lost.

Instead of rotating the second crystal, the crossed crystal configuration could be realized with a half-wave plate (HWP) between the two crystals. If the half-wave plate is chosen correctly, the polarization from photon pairs generated in the first crystal is changed from vertical to horizontal and the polarization of the pump light remains diagonal. To eliminate the disadvantage of having a second crystal, it can be exchanged with a mirror and the half-wave plate with a quarter-wave plate, leading to the folded sandwich configuration [SRJ+13].

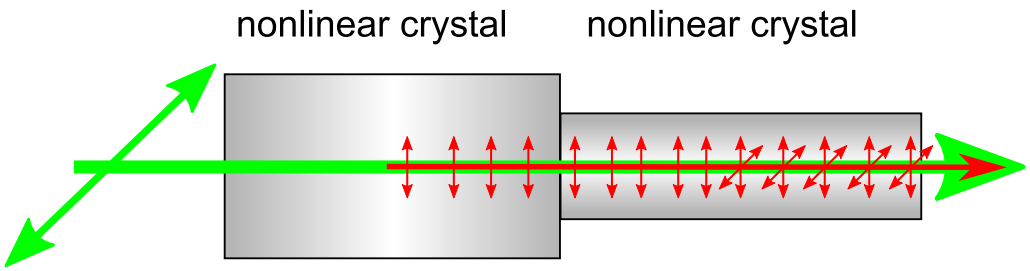

Figure 8: Schematic of the crossed crystal configuration. It consists of two identical nonlinear crystals arranged so that the optical axes of the crystals are orthogonal to each other. The diagonally polarized pump light can generate vertically polarized photon pairs in the first crystal or horizontally polarized photon pairs in the second crystal via type-0 SPDC.

2.3.2 Folded sandwich

The folded sandwich configuration was presented by Steinlechner *et al.* in 2013 [SRJ+13]. Instead of using two nonlinear crystals the folded sandwich configuration uses only one nonlinear crystal. Figure 9 shows the folded sandwich configuration, which consists of a nonlinear crystal, a specifically tailored wave plate and a concave mirror.

The vertically polarized pump light is focused to the middle of the nonlinear crystal and generates vertically polarized photon pairs with a type-0 SPDC process. Since the pump light is focused to the middle of the crystal, it is assumed that the SPDC processes occurs there. The generated photon pairs and the most of the pump light propagate through the nonlinear crystal until they reach the specifically tailored wave plate, which acts as a quarter-wave plate for the generated photons and as a half-wave plate for the pump light. That wave plate changes the polarization of the pump light from vertical to horizontal and the polarization of the generated photon pairs from vertical to circular. A concave mirror is placed behind the wave plate to focus the light back to the middle of the nonlinear crystal. The light will interact a second time with the wave plate, changing the polarization of the pump-light back to vertical and the polarization of the generated photon pairs from circular to horizontal. The SPDC process can occur again in the second pass through the nonlinear crystal and can produce vertically polarized photon pairs.

In summary, one horizontally (first pass generated) or one vertically (second pass generated) polarized photon pair can be found behind the folded sandwich configuration. This is the same result as in the crossed crystal configuration from Section 2.3.1 without the disadvantage of using two nonlinear crystals.

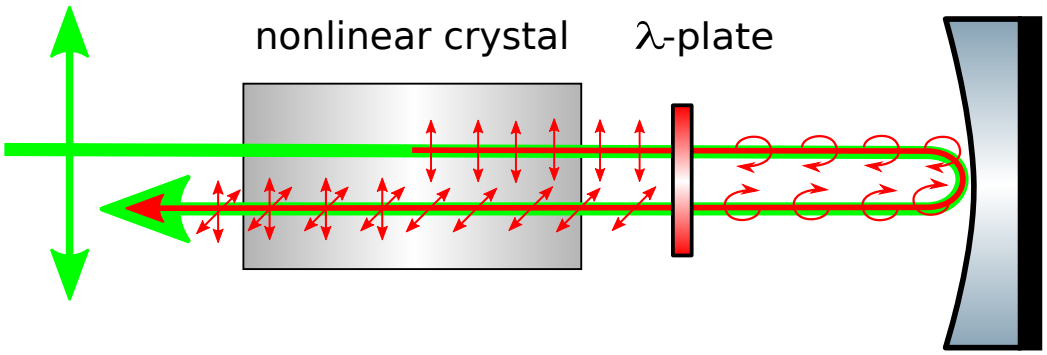

Figure 9: Folded sandwich configuration. It consists of a periodic poled nonlinear crystal, a wave plate with a tailored wavelength dependency and a concave mirror. The wave plate acts like a half-wave plate on the pump light and as a quarter-wave plate on the generated photons. The pump light crosses the nonlinear crystal twice and has a certain probability of generating vertically polarized photon pairs each time. Due to the wave plate, the polarization of the photons generated during the first pass through the nonlinear crystal changes from vertical to horizontal after passing the wave plate twice. Therefore, the folded sandwich configuration produces vertically or horizontally polarized photon pairs. The mirror focuses the light along the original path, the curved path is only for clarity.

3 Experimental setup

The folded sandwich scheme [SRJ+13] is a highly efficient source for polarization entangled photon pairs. The original folded sandwich scheme is wavelength dependent, which is a disadvantage for creating a highly non-degenerated entangled photon pair source. That is why a replacement of the wavelength dependent components was necessary. The tunable entangled photon pair source is shown schematically in Figure 10.

The focusing lens L1 focuses the diagonally polarized pump light (532 nm continuous wave laser) inside a nonlinear crystal. This 40 mm long periodically poled lithium niobate (PPLN) crystal is doped with $\sim 5\%$ magnesium oxide (MgO:PPLN). The pump photons spontaneously split into photon pairs of longer wavelength (see Section 2.1.2) inside the PPLN crystal. The phase matching condition is chosen in such a way that all involved photons are vertically polarized (type-0 phase matching). The probability of SPDC can be maximized by optimizing the focus of the lens L1. The Fresnel rhomb behind the PPLN is oriented at 45°, so that it acts like a quarter-wave plate for the vertically polarized photon pairs. However, the Fresnel rhomb does not modify the polarization of the diagonally polarized pump light. A more detailed explanation of the Fresnel rhomb is given in Section 3.1. A concave mirror (CM) after the Fresnel rhomb reflects the light back into the Fresnel rhomb. This means that the initially generated photon pairs pass through the Fresnel rhomb twice, which results in a overall change from vertical to horizontal polarization. The concave mirror position is optimized to reflect the light back along the original optical path to achieve a symmetric configuration. During the second pass through the PPLN crystal the pump light can again generate vertically polarized photon pairs. The polarization of a pair behind the folded sandwich configuration is horizontal (generated in the first pass) or vertical (generated in the second pass). The probability to find two pairs behind the folded sandwich configuration at the same time is almost zero because of the low intensity of the pump laser.

The longer path in the setup for the first generated photon pairs leads to a different dispersion between first and second pass generated photon pairs. The coherence length of the laser exceeds the length of the setup so that the photon pairs can be distinguished only by their dispersion and polarization. The dispersion information is removed by using birefringent Yttrium orthovanadate (YVO_4) crystal slabs to compensate the difference in the dispersion between the two sets of generated photon pairs. The different dispersion and the need for a compensation crystal will be discussed in Section 3.2. Once the dispersion information has been eliminated, the photon pairs generated in the first and second pass can only be distinguished by their polarization. Hence they are entangled.

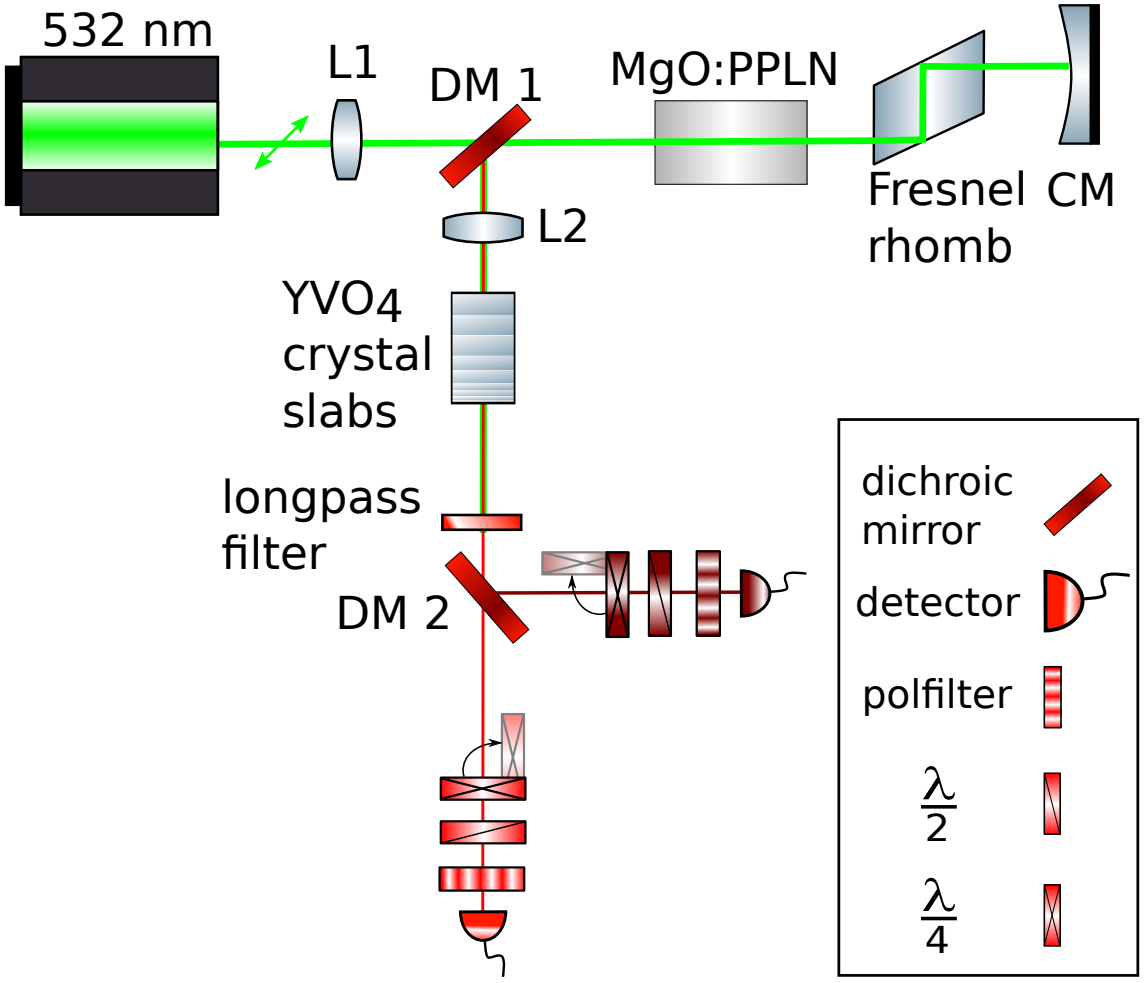

Figure 10: Entangled photon pair source in the modified folded sandwich configuration. The entangled photon pairs are generated in a periodically poled lithium niobate crystal containing $\sim 5\,\%$ magnesium oxide (MgO:PPLN). The generated wavelength can be tuned by adjusting the crystal temperature using an oven (not shown). The continuous wave pump light focused by lens L1 propagates through both the nonlinear crystal and a Fresnel rhomb and is reflected back at a concave mirror (CM). An SPDC process in the nonlinear crystal generates vertically polarized photon pairs. A photon pair generated during the first pass through the nonlinear crystal becomes horizontally polarized after passing through the rhomb, which acts like a quarter-wave plate. A photon pair generated during the second pass remains vertically polarized. The dichroic mirror DM 1 separates the pump and generated photons. Birefringent YVO_4 crystal slabs compensate the dispersion information between the first and second pass generated photon pairs so that the pairs are now polarization-entangled. Lens L2 collimates the generated photons and, finally, a second dichroic mirror DM 2 separates the entangled signal and idler photons.

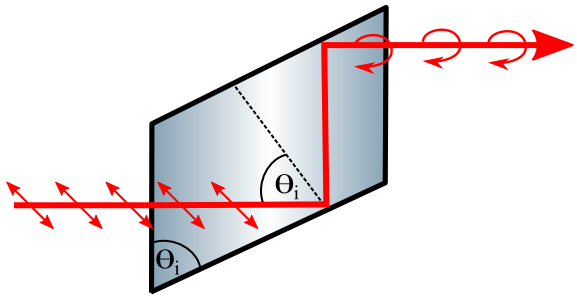

Figure 11: Schematic of a Fresnel rhomb. The incident light is diagonally polarized and the incident angle Θ_i is greater than the critical angle. The total internal reflection in the rhomb leads to a phase shift between s and p polarization of the light. After two reflections the polarization of the light is changed from linear to circular.

The state after the compensation crystal can be described by

$$|\Psi\rangle\,(\lambda_s, \lambda_i) = \frac{1}{\sqrt{2}}\left(|V_{\lambda_s} V_{\lambda_i}\rangle + e^{i\phi(\lambda_s,\lambda_i)}\,|H_{\lambda_s} H_{\lambda_i}\rangle\right) \tag{3.1}$$

where the phase $\phi(\lambda_s, \lambda_i)$ can be adjusted with the compensation crystal, making it possible to obtain the Bell state $|\Phi^+\rangle$ or $|\Phi^-\rangle$ with this setup.

The dichroic mirror DM 1, placed between the lens L1 and the PPLN crystal, transmits the pump photons but reflects the generated photon pairs so that the generated photon pairs propagate to the lens L2. This lens, coated for the SPDC wavelengths, collimates the generated photon pairs. However, DM 1 reflects some of the pump photons too, which is why a longpass filter is placed behind the compensation crystal. Finally, a second dichroic mirror DM 2 separates the signal and idler photons so that these photons can be measured with a detector optimized for their wavelength. In future experiments the polarization analysis will be removed so the created photons can interfere with other quantum systems and establish communication between them.

3.1 Fresnel rhomb

A Fresnel rhomb, depicted in Figure 11, is a glass prism that converts linearly polarized light into circularly polarized light [Hec09]. That means that the function of a Fresnel rhomb is quite similar to a quarter-wave plate. However, a Fresnel rhomb does not use the retardation effect of a birefringent material like a quarter-wave plate. Instead, the Fresnel rhomb uses total internal reflection to cause a phase shift in the two polarization components of the light. The advantage of the Fresnel rhomb is that, in contrast to a quarter-wave plate, the phase shift is almost wavelength independent.

There are super achromatic wave plates which are quite wavelength independent over a broad range, but their range is limited in comparison to a Fresnel rhomb [Die15]. It is possible to tailor a wave plate exactly for a special wavelength range

but this would limit the tunability of the source as well. That is why a Fresnel rhomb was chosen instead of a super achromatic wave plate.

The Fresnel rhomb relies on a phenomenon known as total internal reflection to change the polarization of the light. Total internal reflection refers to the complete reflection of light at an interface between media with different refractive indices [ST08]. This phenomenon occurs when the material after the interface has a lower refractive index and the incident angle Θ_i of the light is larger than the critical angle

$$\Theta_c = \arcsin\left(\frac{n_2}{n_1}\right) \tag{3.2}$$

where n_1 and n_2 are, respectively, the refractive indices of the media before and after the interface. In the case of the Fresnel rhomb used for this setup, air is the medium with the lower refractive index n_2 and BK7 glass is the medium with the higher refractive index $n_1 = n_1(\lambda)$. The phase shift ϕ between s and p polarization of a wave caused by a total internal reflection

$$\phi = 2\arctan\left(\sqrt{\frac{\cos^2(\Theta_c)}{\cos^2(\Theta_i)} - 1}\right) + 2\arctan\left(-\frac{1}{\sin^2(\Theta_c)}\sqrt{\frac{\cos^2(\Theta_c)}{\cos^2(\Theta_i)} - 1}\right) \tag{3.3}$$

depends on the critical angle Θ_c and the incident angle Θ_i. The phase shift after one total internal reflection in the rhomb is 45°, which leads to a change in the polarization from linear to elliptical. A second reflection gives an additional phase shift of 45° and transforms the elliptical polarization to circular. Overall, this means that the polarization is changed from linear to circular. If the light is horizontally (or vertically) polarized, then it has only an s (or p) polarization component. A phase shift between an existing s (or p) polarization and non-existing p (or s) polarization component cannot occur. The result is that the Fresnel rhomb will not change the polarization of vertically or horizontally polarized light. The consequence is that the incident wave has to be diagonally polarized to change the polarization from linear to circular.

The Fresnel rhomb in the setup from Figure 10 is rotated by 45°, so that the diagonal polarization of the pump light is not modified. The polarization of the generated photon pairs is changed from vertical to horizontal after passing through the Fresnel rhomb twice.

The refractive index of BK7 for a 894.3 nm photon is 1.5086 [Mes08], which yields with Equation (3.2) a critical angle of 41.5°. The Fresnel rhomb in the setup is cut for an angle of incidence of 54.8°. Using this with Equation (3.3) leads to a phase shift of 44.8° for 894.3 nm photon after one total internal reflection. The total phase shift by passing the rhomb is then 89.6° which differs from the desired 90°. However, this error is negligible compared to the uncertainty from manually rotating the Fresnel rhomb to 45°.

3.2 Compensation crystal

The compensation crystal is necessary in this setup to erase the information regarding which pass through the nonlinear crystal the photon pair was generated in. Figure 10 shows that the compensation crystal is placed behind the generation scheme which consists of the nonlinear crystal, Fresnel rhomb and a concave mirror. The reason for this compensation is that the photon pairs are generated at different locations and therefore accumulate different dispersion in the setup.

It is assumed that the photon pairs are generated in the middle of the nonlinear crystal because that is where the pump light is focused to. The pump light generates photon pairs during the first pass through the nonlinear crystal. These pairs accumulate phase as they pass from the middle of this crystal to its end (extraordinary axis), twice through the Fresnel rhomb and back through the whole length of the nonlinear crystal (ordinary axis). This is in contrast to the pairs generated in the second pass, which only accumulate phase from the middle of the nonlinear crystal to its end. The different wavelength dependent phase accumulation leads to different dispersion between the first and second pass generated photon pairs. The difference in the path for the first and second pass generated photons is illustrated in Figure 12. The phase difference between the first and second pass generated photon pairs is

$$\Phi(\lambda_s, \lambda_i) = 2\pi \left[L_{PPLN} \left(\frac{n^o_{PPLN}(\lambda_s, T)}{\lambda_s} + \frac{n^o_{PPLN}(\lambda_i, T)}{\lambda_i} \right) + 2L_{Rhomb} \left(\frac{n_{BK7}(\lambda_s)}{\lambda_s} + \frac{n_{BK7}(\lambda_i)}{\lambda_i} \right) \right] \tag{3.4}$$

where L_{Rhomb} is the length of the rhomb, L_{PPLN} is the length of the PPLN crystal, λ_s is the wavelength of the signal photons, λ_i the wavelength of the idler photons, n^o_{PPLN} the ordinary refractive index of the PPLN crystal and n_{BK7} is the refractive index of the Fresnel rhomb. In the following discussion it is assumed signal and idler photons have the wavelengths of 894.3 nm and 1313.1 nm.

The result of the different dispersion is that the photon pairs are distinguishable which diminish the entanglement. Figure 13 shows the envelope of photon wave packets with different propagation lengths in a dispersive material. This shows that it is possible to distinguish them with time resolved measurements. That is why it is important that both photon pairs ultimately have in the end the same dispersion to obtain entanglement with that setup.

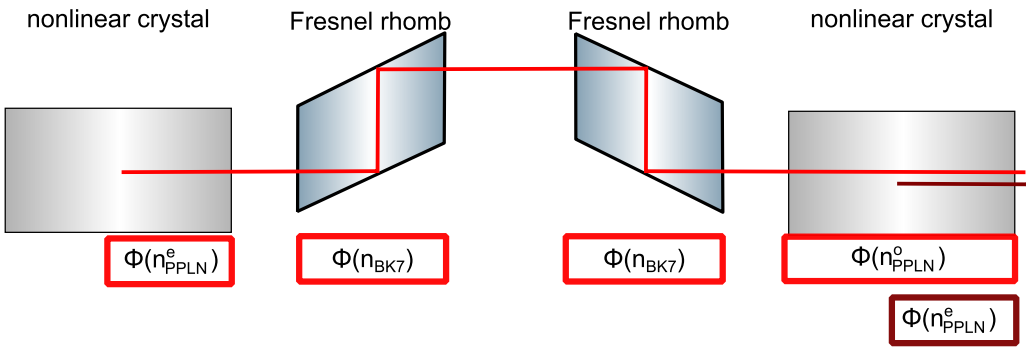

Figure 12: Part of the setup from the point of view of the generated photon pairs. It is assumed that the photon pairs are generated in the middle of the nonlinear crystal. The first pass generated photon pairs (red) accumulate phase in half of the nonlinear crystal (extraordinary axis), twice the length of the path through the rhomb and the whole length of the nonlinear crystal (ordinary axis). In contrast, the photon pairs which are generated in the second pass through the nonlinear crystal (brown) accumulate phase in half of the nonlinear crystal (extraordinary axis). The result is that the photon pairs generated in the first pass accumulate a different wavelength dependent phase, leading to dispersion. That is why it is possible to determine the generation location by the dispersion which decreases the entanglement in this setup. The phase difference for the first and second pass generated photon pairs can be described with Equation (3.4).

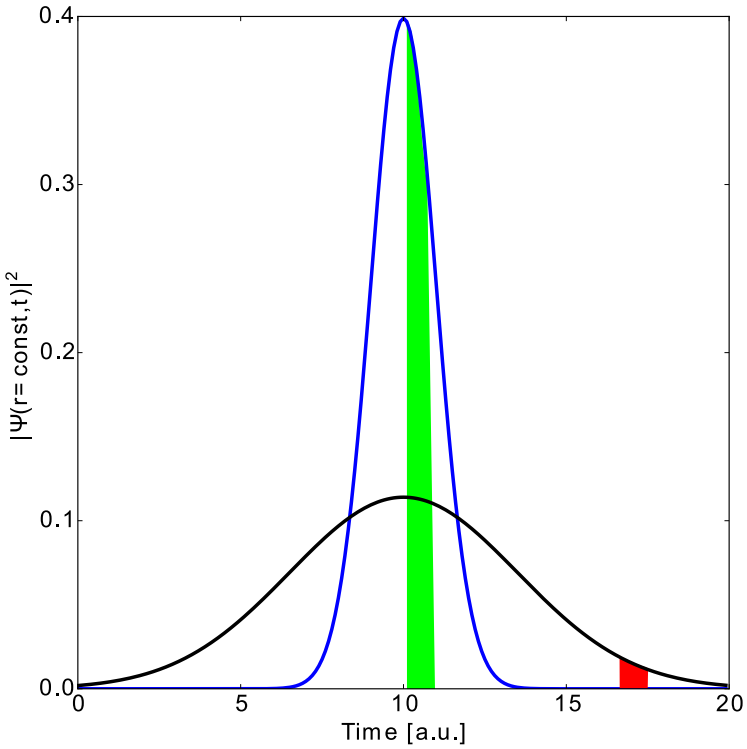

Figure 13: Different envelopes of a photon wave packet caused by dispersion. It is assumed that the incident photon is a Gaussian pulse. The blue and black line show the envelope of a photon after a short and a large distance through a dispersive material, respectively. For shorter time regimes (green box) either photon is likely to be detected. However, after a longer time (red box) the probability of detecting the photon that has traveled the longer path trough the dispersive medium is much higher. The consequence of the different dispersions is that the photons can be distinguished by a time resolved measurements.

The approach to equalizing the dispersion is to use an additional birefringent crystal. That is possible because the first and second generated photon pairs have a different polarization. The birefringent crystal is placed in the setup in that way that horizontal polarization has the lower refractive index and the vertical polarization has the higher refractive index. The result is that the photon pairs which are generated in the second pass accumulate more phase in the compensation crystal than the photon pairs generated in the first pass through the nonlinear crystal. The fidelity and thus the entanglement is very sensitive to the optimal compensation crystal length. If the compensation crystal is too short, then there is still dispersion between first and second pass generated photon pairs. However, if the compensation crystal is too long, then the second pass generated photon pairs are now affected by the higher dispersion and the photon pairs are again distinguishable. The requirements for the compensation crystal are low losses in the visible and near infrared light and a large difference between the refractive indices of ordinary and extraordinary axis. This leads to a shorter compensation crystal length. A material which has a large difference in the refractive index and only few losses is Yttrium orthovanadate (YVO_4) [Foc15]. For this crystal the phase difference between both polarizations is

$$\tilde{\Phi}(\lambda_s, \lambda_i) = 2\pi L_{YVO_4} \left[\frac{\Delta n_{YVO_4}(\lambda_s)}{\lambda_s} + \frac{\Delta n_{YVO_4}(\lambda_i)}{\lambda_i} \right] \tag{3.5}$$

where L_{YVO_4} is the length of the compensation crystal and Δn_{YVO_4} the difference in refractive index between ordinary and extraordinary axis.

It is possible to calculate the length of the compensation crystal with Equation (3.4) and Equation (3.5) so that the phase fulfills the so-called flat phase condition

$$\frac{d}{d\lambda} \left(\Phi(\lambda_s, \lambda_i) + \tilde{\Phi}(\lambda_s, \lambda_i) \right) \Big|_{\lambda_s, \lambda_i} \approx 0. \tag{3.6}$$

With that the dispersion of the first and second pass generated photon pairs are equal. Equation (3.6) shows that a constant offset is irrelevant for compensating the dispersion for the signal and idler photons of both pairs.

For calculating the optimal compensation crystal length it is necessary to know the refractive index difference of YVO_4. The equation which gives the wavelength dependent refractive index of a material is the Sellmeier equation. However, there are different Sellmeier equations for YVO_4 in the literature, and each one yields a different optimal length for the compensation crystal [Foc15; ZLC+10; ST14; BDE+09]. Furthermore, the refractive indices for the nonlinear crystal [GSG+08] and of the Fresnel rhomb [Mes08] are important to know the phase, which has to be compensated. The optimal compensation crystal lengths for the signal wavelength of 894.3 nm and idler wavelength of 1313.1 nm are shown in Table 3. The needed length of the compensation crystal depends on the wavelength of the idler and signal photons as well. Figure 14 shows that different compensation crystal lengths

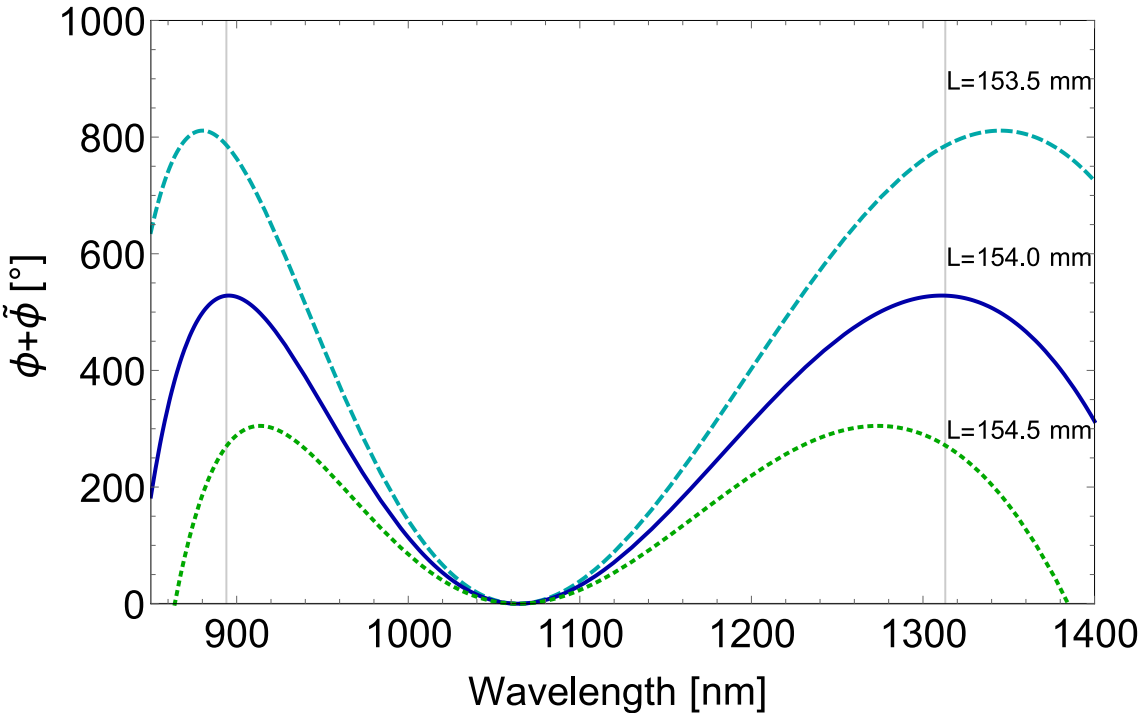

Figure 14: Compensated phase for different crystal lengths according to Equation (3.4) and (3.5). From Equation (3.6) it is known that the dispersion is equal if there is an extremum in the function. The position of the extremum changes for small variations of compensation crystal length. This means that the dispersion is compensated for different signal and idler wavelengths. If the crystal is too long or too short, then the phase cannot be compensated for any wavelength. A constant offset is subtracted so that the phase is zero in the case of degenerate signal and idler photons. The refractive indices from Zelmon *et al.* [ZLC+10] were used to calculate these functions.

compensate different wavelengths for the signal and idler photons. The optimal length for a given wavelength is achieved when the relative phase is flat (see Equation (3.6)). That means that the derivative of the phase (dispersion) will vanish and it is impossible to distinguish the photon pairs by their dispersion. The YVO_4 crystal in this the setup is not a single crystal but consists of several slabs with different thicknesses. The compensation crystal length needed in the setup can be determined by measuring the entanglement. Furthermore, it is possible to get the optimal length for other wavelength combinations as well if slabs can be added and removed. The thinnest slab is 0.2 mm thick but the setup is not limited by that thickness. Instead of adding smaller slabs it is possible to temperature tune parts of the compensation crystal, which will be discussed in the following.

Two changes occur when the crystal is heated. The crystal becomes longer due to thermal expansion and the optical properties of the crystal change with the temperature. The material dependent thermal expansion coefficient α is defined as

$$\alpha = \frac{1}{L}\frac{dL}{dT} \tag{3.7}$$

where L is the length of the material and T the temperature. In the case of linear

Table 3: Optimal compensation crystal lengths using different Sellmeier equations for YVO_4 from four different references. The optimal lengths were calculated for a signal wavelength of 894.3 nm and a idler wavelength of 1313.1 nm. The variation of the refractive index difference $\Delta n = n_e - n_o$ for YVO_4 in the references was quite small but led to a significant difference in the optimal compensation crystal length. The Sellmeier equations from the different references are given in Appendix A.

crystal length	Δn_s	Δn_i	reference
138.7 mm	0.211014	0.205271	Foctek Photonics Inc. [Foc15]
154.0 mm	0.211408	0.205448	D. Zelmon *et al.* [ZLC+10]
172.0 mm	0.211750	0.205685	Y. Sato *et al.* [ST14]
178.8 mm	0.209959	0.204678	Handbook of Optics [BDE+09]

thermal expansion, the thermal expansion coefficient α can be approximated as a constant and the length at a given temperature is given by

$$L(\Delta T) = L_0(1 + \alpha \Delta T) \tag{3.8}$$

where L_0 is the initial length. An expansion of the crystal leads to an increased phase accumulation. Furthermore, the refractive index of a material changes by heating the material

$$n(\Delta T) = n_0 + \epsilon \Delta T \tag{3.9}$$

where n_0 is the primary refractive index and ϵ the, generally wavelength dependent, thermal optical coefficient. The refractive index of YVO_4 increases with increasing temperature [ST14]. There are different values for the thermal optical coefficients of YVO_4 in the literature [ST14; Foc15], but they all agree that the ordinary axis increases more than the extraordinary axis. This results in a decreasing refractive index difference between ordinary and extraordinary axis at a higher temperature for YVO_4

$$\Delta n_{YVO_4}(\Delta T) = \Delta n_0 - \Delta\epsilon \Delta T \tag{3.10}$$

where Δn_0 is the primary refractive index difference of the ordinary and extraordinary axis and $\Delta\epsilon$ the positive thermal optical coefficient for both refractive indices. The difference of the refractive indices Δn in YVO_4 decreases with increasing temperature, leading to a lower compensation of this crystal (see Equation (3.5)). The total change for the phase ϕ can be obtained as

$$\begin{aligned}\Delta\phi(\Delta T) = 2\pi L \Bigg[&\frac{\Delta\epsilon_s \Delta T + \alpha \Delta T(\Delta n_s - \Delta\epsilon_s \Delta T)}{\lambda_s} + \\ &\frac{\Delta\epsilon_i \Delta T + \alpha \Delta T(\Delta n_i - \Delta\epsilon_i \Delta T)}{\lambda_i} \Bigg]\end{aligned} \tag{3.11}$$

where Δn_s and Δn_i are the refractive index difference between the ordinary and extraordinary axes for the signal and idler wavelengths, respectively, $\Delta\epsilon_s$ and $\Delta\epsilon_i$ are the positive thermal optical coefficients of Δn_s and Δn_i.

The dominant effect is the temperature dependence of the refractive index, leading to less phase accumulation of the compensation crystal at higher temperature. That is in a good agreement with a measurement for YVO_4 at a wavelength of 894.3 nm [Wei]. This different phase accumulation can be used to change the phase ϕ of the generated entangled state, shown in Equation (3.1), to yield a Bell state. The temperature needed to obtain a phase shift of π is particularly interesting since a phase shift of π enables switching between the Bell states $|\phi^+\rangle$ and $|\phi^-\rangle$. In the setup 3 cm of the compensation crystal are placed in an oven and can be heated. The result from Equation (3.11) is that 1.3 °C are needed to obtain a phase shift of π with the thermal optical coefficient and the refractive index from Sato *et al.* [ST14].

The optimal compensation can be obtained by putting slabs in the setup so that crystal is close to the optimal compensation length. By changing the refractive index of some crystals slabs via heating, the optimal compensation can be achieved.

3.3 Visibility measurement

A high visibility

$$v = \frac{N_{max} - N_{min}}{N_{max} + N_{min}} \tag{3.12}$$

in each basis is also evidence for entanglement [WGP+07] (see Section 2.2.2). The minimum and maximum number of coincidence counts can be obtained by rotating the half-wave plate in the signal arm (see Figure 10). If the visibilities in each basis are measured, it is possible to calculate the entanglement fidelity from Equation (2.63).

The photon source provides vertically and horizontally polarized photons. This results in a high visibility in the horizontal and vertical basis because the coincidence counts between horizontally and vertically polarized photons should be zero. The coincidence counts will oscillate when an half-wave plate placed before the polarization filter is rotated. The coincidence counts reach a maximum when the measured bases are equal and a minimum when the bases are perpendicular to each other. This is a classical expectation and has nothing to do with entanglement. The expectations for the other bases are different. If the signal arm is fixed to the diagonal polarization basis, then rotating the half-wave plate in the idler arm should not change the coincidence counts. The same is true for the anti-diagonal, left and right circular polarization bases. Constant coincidence counts leads to a visibility of zero. However, if the photons are entangled there will be an oscillation in all bases as in the horizontal or vertical basis depending on the position of the half-wave plate. The needed position of the wave plates to project to different polarization bases are given in Table 4.

Table 4: Projection in different polarization bases. The polarization filter in each arm (see Figure 10, for the polarization optics) is fixed to 90°. The half-wave plates before the polarization filters are used to change the measured polarization. The half-wave plate in the signal arm is fixed during a measurement while the half-wave plate in the idler arm is rotated to measure the coincidence counts for different half-wave plate positions. An additional quarter-wave plate is used in each arm to achieve circular polarization. The different orientations of the retardation plates are needed to measure in the different polarization bases.

	signal arm		idler arm
basis	Θ_{HWP}	Θ_{QWP}	Θ_{QWP}
V	45°	-	-
H	0°	-	-
D	-22.5°	-	-
A	22.5°	-	-
R	0°	-45°	-45°
L	0°	45°	45°

In summary, a non-zero visibility in the diagonal, anti-diagonal, left circular or right circular basis is evidence for entanglement. It would be enough to measure the maximum and minimal coincidence counts by rotating a half-wave plate in one arm to determine the visibility. However, for a better statistical result the coincidence counts for several half-wave plate positions are measured and the visibility is then calculated. Figure 15 shows the comparison between a entangled and non-entangled state by such a measurement.

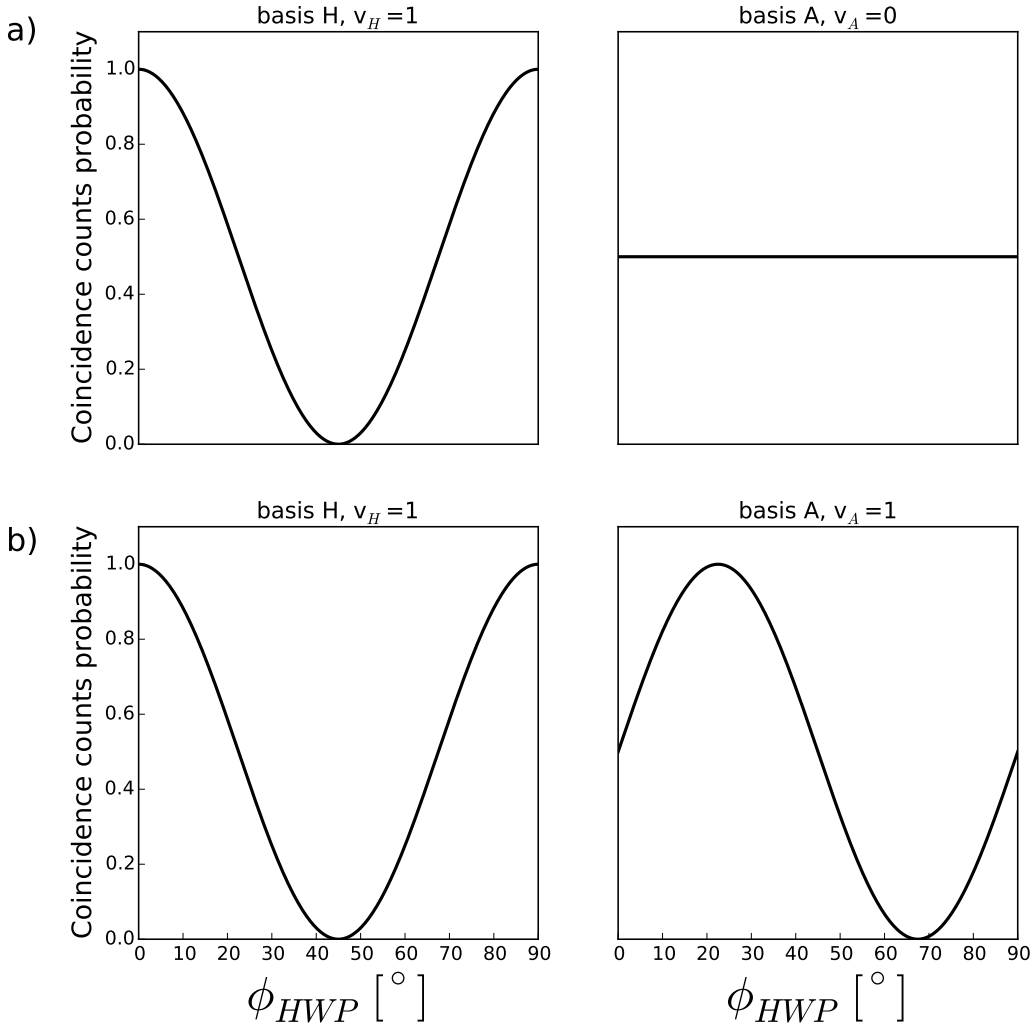

Figure 15: Expected results of a visibility measurement. For a) non-entangled, classically correlated horizontally or vertically polarized photon pairs. The oscillation in the horizontal basis is a sine function which goes down to zero, leading to a visibility of 1. The expectation in the anti-diagonal basis is a constant value because of the independent measurement projection to one state for each arm. The result is that the visibility in that basis is 0. The b) Bell state $|\phi^+\rangle$ has the same expectation in the horizontal basis like non-entangled state. However, there will be also an oscillation in the anti-diagonal basis. Ideally, this oscillation goes down to zero, yielding a visibility of one. The expectation for the vertical basis for both cases is equal to the horizontal basis with a phase shift of 45°. In the diagonal, right circular or left circular basis will be also a constant value for the non-entangled state. However, for the bases in the Bell state $|\phi^+\rangle$ there will be an oscillations as shown for the anti-diagonal basis in b) but with a different phase shift in each basis.

4 Results

This chapter presents the results of this thesis. First the tunability of the generated photon pairs will be shown in Section 4.1. The optimal compensation crystal length is determined in Section 4.2. Then the fidelity of the setup can be measured, which is discussed in Section 4.3. Finally, Section 4.4 shows that it is possible to change the generated state by tuning the compensation crystal temperature.

4.1 Tunability

The wavelengths of the signal and idler photons depend on the nonlinear crystal and the pump wavelength λ_p. The wavelength of the idler λ_i photons can be calculated for a given signal photon wavelength λ_s with

$$\lambda_i(\lambda_s) = \left(\frac{1}{\lambda_p} - \frac{1}{\lambda_s}\right)^{-1}, \tag{4.1}$$

which is another formulation of the energy conservation from Equation (2.6). Figure 16 shows the theoretical relationship between the wavelength of the signal and idler photons for a pump wavelength of 532 nm. This theoretical curve is in a good agreement with experimental results [Kre].

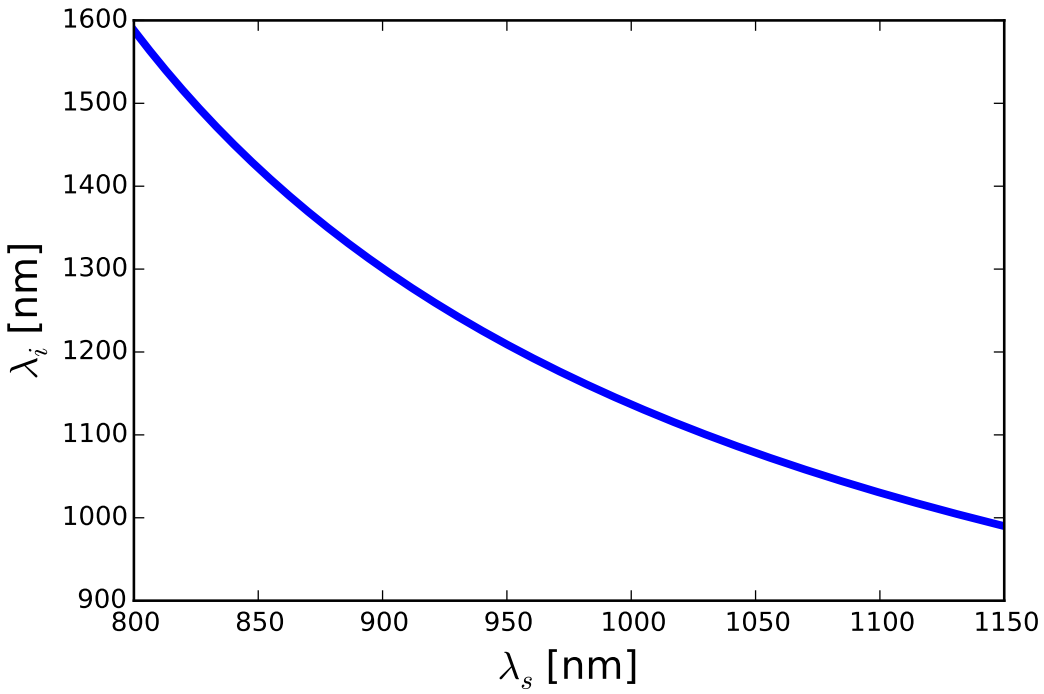

Figure 16: Theoretical relationship between signal and idler wavelengths for a pump wavelength of 532 nm according to Equation (4.1).

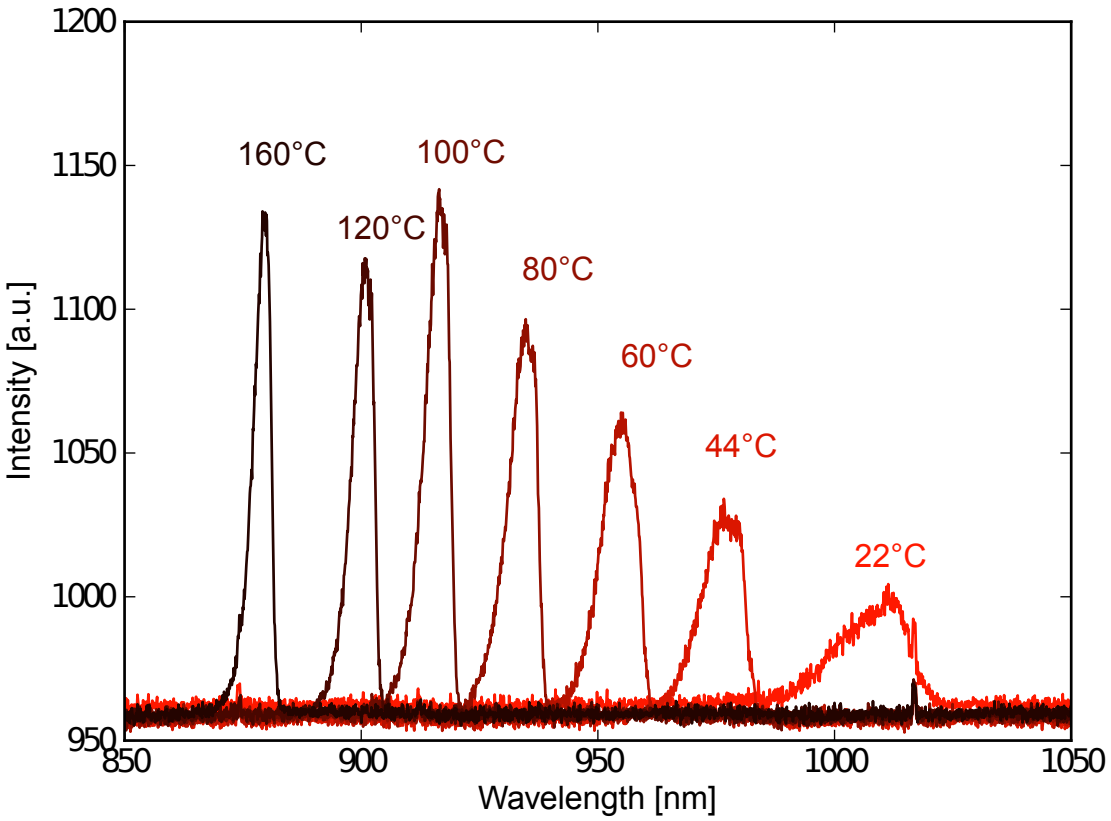

Figure 17: Signal photon spectra for different temperatures of the PPLN crystal. Decreasing intensity is due to the detection probability of the spectrometer. Changing the crystal temperature often requires readjustment of the mirrors. That is why the intensity at 120 °C is lower than the intensity at 100 °C and 160 °C. Image adapted from [Die15].

Heating the nonlinear crystal changes the quasi-phase matching condition, given by Equation (2.11), which changes the wavelength of the generated photon pairs. The nonlinear crystal in this setup can be heated up to 160 °C. The wavelengths of the signal photons generated using the 7 µm grating in the nonlinear crystal at different temperatures are shown in Figure 17. This grating has a tuning range from 870 nm to 1100 nm for the signal photons and 1124 nm to 1345 nm for the idler photons. Other gratings can be chosen to achieve a higher tuning range.

The crystal is heated to 133.4 °C to obtain 894.3 nm signal photons, which is the wavelength of the cesium D1 line [Ste08]. Figure 18 shows the spectra of the signal photons generated during the first and second passes through the nonlinear crystal. It is of paramount importance that the spectra of both passes are identical, otherwise the photons are distinguishable and the entanglement is ruined. It can be assumed, due to energy and momentum conservation, that if the spectra for the signal photons are identical, then the spectra of the idler photons are also identical. The folded sandwich configuration has to be aligned very precisely to obtain the same spectrum for the first and second pass generated photons. If the beam paths of the first and second passes differ, then it is possible to obtain slightly different

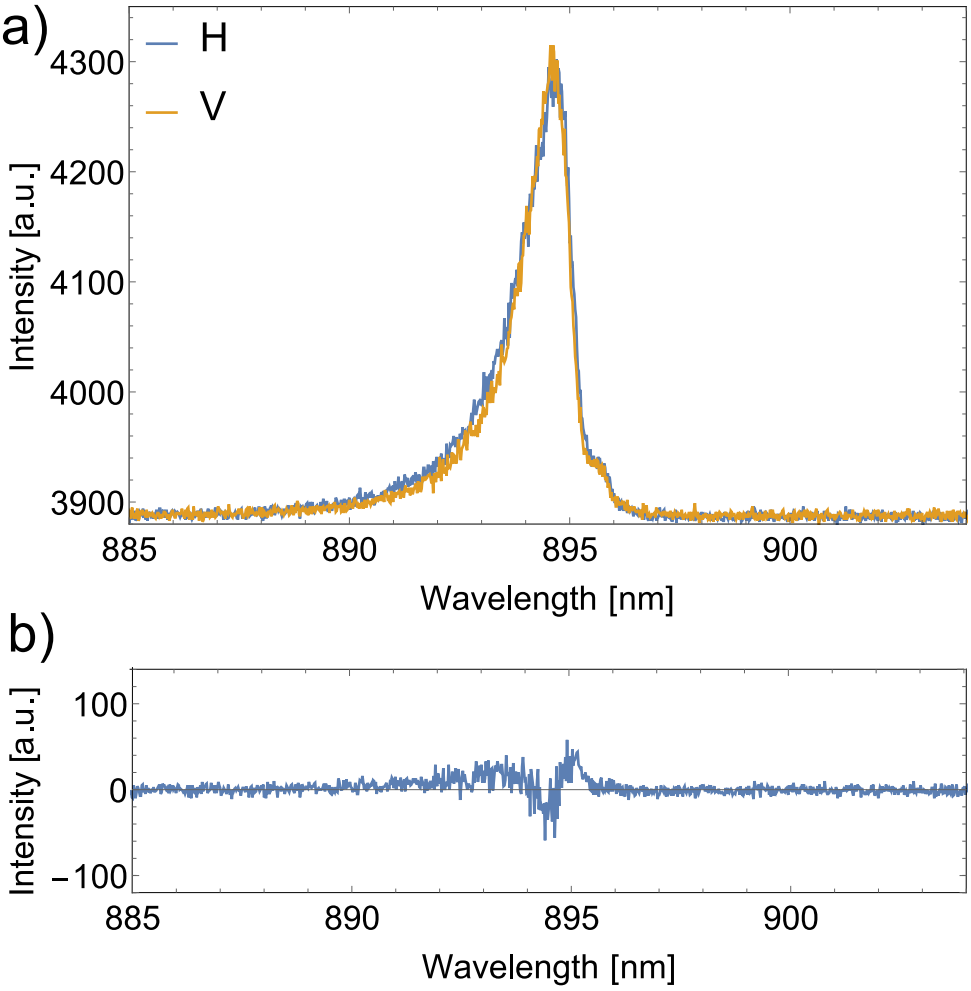

Figure 18: Spectra of the signal photons with vertical and horizontal polarization. a) The different polarizations are used to compare the photons that are generated in the first (vertical) and second (horizontal) pass. The spectra of the two passes through the nonlinear crystal are almost identical. The spectral width of the photons is approximately 1.5 nm. b) Difference of the vertically and horizontally polarized signal photons. Note the different magnitude of the y-axis.

wavelengths for the vertically and horizontally polarized photon pairs. The reason is that if the beam propagates through the nonlinear crystal with a different incident angle, then the effective grating of the quasi-phase matching is longer, leading to a different wavelength.

The polarization of the pump light is changed with a half-wave plate so that the intensity of the signal photons generated in the first and second pass are equal, as shown in Figure 18. The Bell states, which are the maximally entangled two photon states, require that the photons have the same wavelength and intensity. As a result, it is also important to have the same wavelength and intensity for the first and second pass generated photon pairs for a high fidelity.

4.2 Optimal compensation crystal length

The optimal compensation crystal length is found by measuring the visibility in the left circular basis. This means that the coincidences are measured for left circular polarization fixed in one arm while the half-wave plate in the other arm is rotated, as discussed in Section 3.3. From the coincidence counts the visibility is extracted, as follows. The variation of the coincidence counts N can be assumed as a sine function with an offset C

$$N = A \sin(4\,\phi_{HWP} + \delta) + C \tag{4.2}$$

where ϕ_{HWP} is the position of the half-wave plate in the idler arm, A the amplitude of the oscillation and δ is the phase. The minimum N_{min} and maximum N_{max} of the coincidence counts can be written using the coefficients A and C

$$N_{max} = A + C \qquad N_{min} = -A + C \tag{4.3}$$

and the one-photon visibility can be expressed as

$$v = \frac{N_{max} - N_{min}}{N_{max} + N_{min}} = \frac{A}{C}. \tag{4.4}$$

Examples of visibility measurements for different compensation crystal lengths are depicted in Figure 19. The highest visibility for an 894.3 nm signal photon was obtained with a compensation crystal length of 153 mm. A comparison with Table 3 shows that 153 mm is in a good agreement with the optimal compensation crystal length calculated with the refractive indices from D. Zelmon *et al.* [ZLC+10].

4.3 Fidelity measurement

The visibilities in the six polarization bases are needed to determine the fidelity as discussed in Section 2.2.2. The half-wave plates and quarter-wave plates of the setup are used to measure in the different polarization bases. Table 4 shows the required positions of the retardation plates to project in each polarization basis. The half-wave plate in the idler arm is used to measure the oscillation of the coincidence counts. Measuring the same state gives the maximal coincidence counts

$$N_{ii} = N_{max} \tag{4.5}$$

and measuring two orthogonal states yield the minimal coincidence counts

$$N_{ij} = N_{min}. \tag{4.6}$$

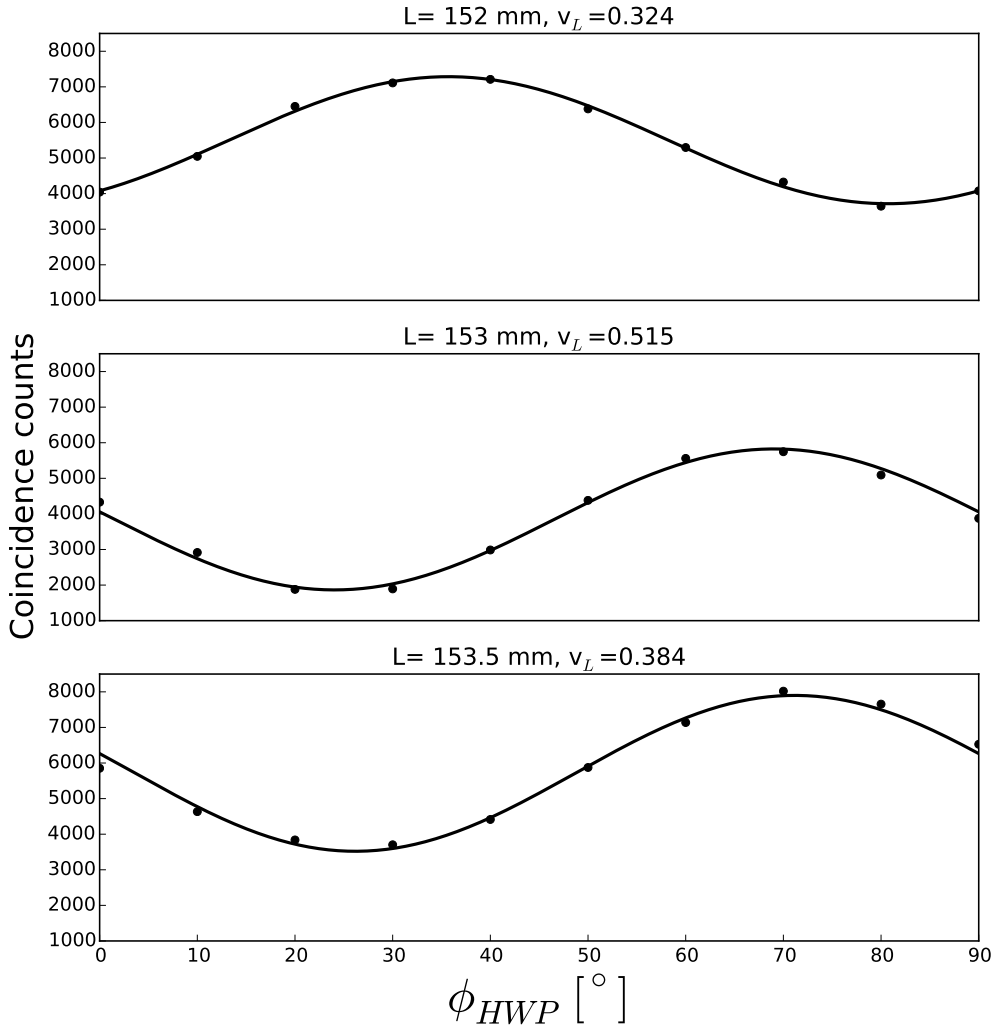

Figure 19: Visibility measurements for different compensation crystal lengths in the left circular basis. The measured points (•) show a sinusoidal behavior, as expected from Equation (4.2). The oscillation of the coincidence with rotation of the half-wave plate is evidence for entanglement. The highest visibility was measured for a compensation crystal length of 153 mm. The different crystal length leads to a change in the coupling, which explains the different coincidence count rates between the measurements.

Equation (2.61) can be rewritten with the coefficients of the nonlinear fit from Equation (4.2) as

$$V_{ij} = \frac{A_i + A_j}{C_i + C_j} \tag{4.7}$$

for the different polarization bases (ij=H/V,D/A,R/L). The measurement of the fidelity with a compensation crystal of 153 mm is shown in Figure 20. The resulting entanglement fidelity is

$$F = (75.3 \pm 2.1)\%.$$

The signal APD has an efficiency of 10 % at 894.3 nm. The raw APD count rate was $\sim$ 215.000 counts per seconds (cps), leading to a corrected count rate of $2.15 \cdot 10^6$. The pump power of the laser was 370 µW, which gives a brightness of 5.8 Mcps/mW. The spectral width of the signal photons is $\Delta\lambda$=1.5 nm (see Figure 18), yielding a spectral brightness of 3.87 Mcps/(mW nm).

4.4 Phase adjustment

The phase ϕ in Equation (3.1) can be changed by varying the compensation crystal length. Every addition or removal of a slab changes ϕ. However, the temperature of the nonlinear crystal also influences ϕ due to the temperature dependence of the optical properties, as discussed in Section 3.2. For fine tuning of the phase ϕ, 30 mm of the compensation crystal are placed in a tunable oven. Figure 21 shows the trend of the coincidence counts while changing the temperature of the oven. The measurement was done in the anti-diagonal basis because this basis has been shown experimentally to have the strongest oscillation caused by entanglement. The result is that a temperature change of approximately 2.4 °C is needed to achieve a phase shift of π in this setup. The needed temperature is higher than the theoretical temperature estimated in Section 3.2. The higher temperature could be explained with a decreasing room temperature during the measurement since 123 mm of the compensation crystal are at room temperature. A temperature stabilization of the compensation crystal will be discussed in detail in the next section.

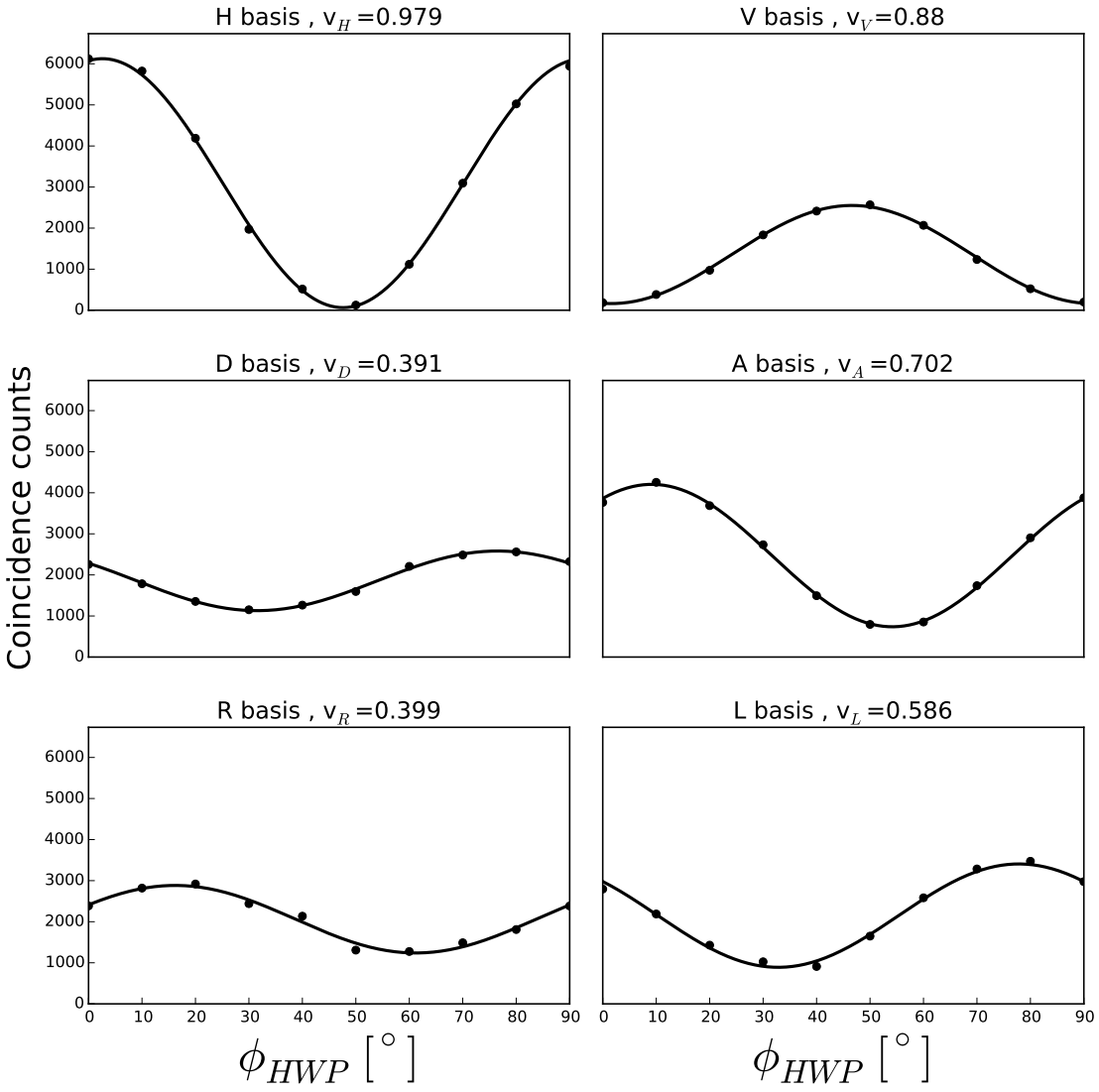

Figure 20: Fidelity measurement with a compensation crystal length of 153 mm. The oscillation in all basis shows that the source indeed generates a (partially) entangled state. The maximal coincidence counts in the vertical basis is lower than in the horizontal basis. This could be evidence that more horizontal polarized reached the detectors because of the losses in the setup. The calculated (Equation (2.63)) fidelity is 0.753±0.21.

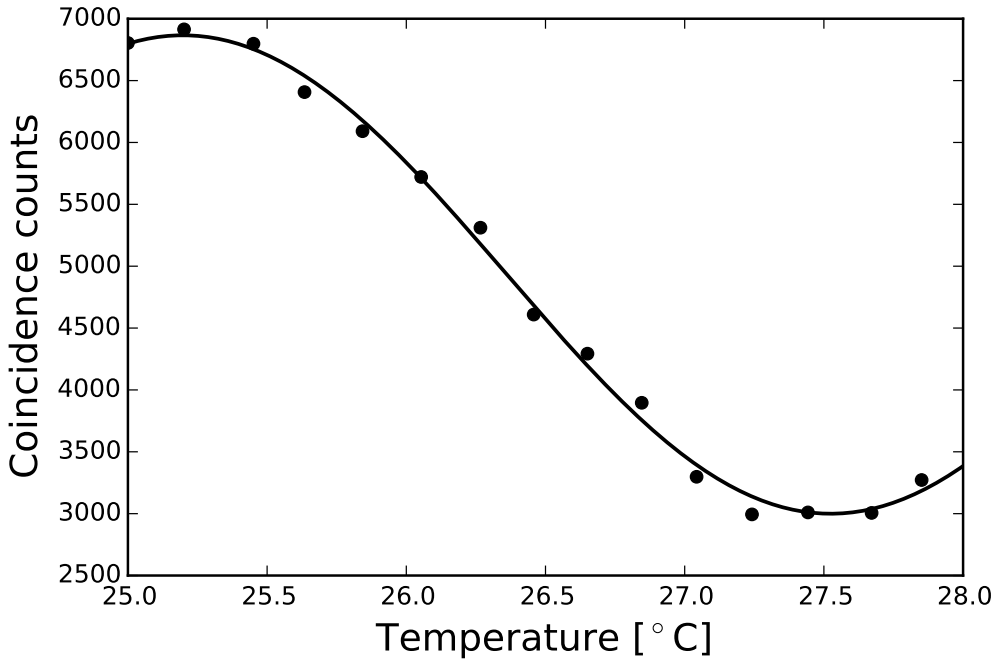

Figure 21: Coincidence counts in the anti-diagonal basis. 30 mm of the compensation crystal are temperature tuned. The variation of the coincidence counts shows the changing of the phase ϕ in the generated state in Equation (3.1). With this mechanism it is possible to switch between the Bell states $|\phi^+\rangle$ and $|\phi^-\rangle$.

5 Conclusion

This thesis presented a modified folded sandwich configuration. Since it is based on a geometrical principle, the wavelength of the generated photons can be changed easily. This proof of principle experiment shows that the source is able to provide entangled photons. The fidelity is currently lower than that obtained from other sources [SRJ+13; HHP+09; TW08], but can be increased by adjusting the focusing parameters. Improving the focusing parameters should also narrow the bandwidth of the generated photons, increasing the spectral brightness of the source.

Another issue is the temperature dependence of the compensation crystal. Only 30 mm of the entire 153 mm compensation crystal is placed in an oven. The remaining 123 mm are at room temperature. If the room temperature varies, then the phase of the setup varies as well. This is detrimental for a fidelity measurement. Steinlechner *et al.* used a compensation crystal of 18.3 mm and they recommended stabilizing their compensation crystal to $\pm$ 0.1 °C to achieve a fidelity above 99.5% [SRJ+13]. The compensation crystal of the geometrical folded sandwich is almost 8.5 times longer. Therefore, a more accurate temperature control is needed to achieve a fidelity above 99.5%. However, it is now possible to design an oven to enclose the entire compensation crystal since the required crystal length has been determined.

The nonlinear crystal is placed in an oven which is stabilized to 0.1 °C. The detected counts of the generated photon pairs varies with that temperature change. It is interesting that the rate of photons generated in second pass varied more strongly than the rate of photons generated in first pass. It is possible that the temperature variation changes the coupling in the setup, which causes the variation in the detected counts. The different variation for the first and second pairs can be explained by a slightly different focus in the nonlinear crystal, so that the first pass may be more stable with temperature changes. The focusing parameters should be improved to reduce the signal variation.

The maximal coincidence counts vary in each basis during the fidelity measurement (see Figure 20). This means that the probability to obtain a vertically or horizontally polarized photon pair differs. One reason could be the wavelength and polarization dependent losses in the setup. The compensation crystal changed the losses as well through changes in position or length. The polarization dependent losses should be reduced to a minimum by fixing the position of the compensation crystal.

The geometrical folded sandwich configuration is ideally suited for quantum interface applications because it provides entangled photons with different wavelengths.

6 Outlook

The next plans are to increase the fidelity and the spectral brightness of the geometrical folded sandwich configuration.

The spectral brightness can be increased by narrowing the spectral width of the generated photon pairs. The bandwidth of the generated signal photons was calculated in Section 2.1.3 to be 0.37 nm, which correspond with the specification provided by the crystal manufacturer (HC Photonics Corp., personal communication, May, 28, 2015). This theoretical value is smaller than the measured bandwidth of 1.5 nm. The broader spectral width could be caused by sub-optimal focusing parameters in the setup. The focusing was chosen to be quite strong, for efficient conversion. Less focusing leads to a longer collimation range for the beam. Optimally, the beam would be collimated over the entire length of the nonlinear crystal. If the beam is only collimated over part of the crystal length, then the beam cannot interact with the entire periodically poled structure in the nonlinear crystal, which results in a broader spectrum. By optimizing the focus parameters a lower spectral width should be possible. This is important to provide more photons of the wavelength of interest and to match the source to intrinsically narrow transition lines in stationary quantum systems (quantum dots or atomic ensembles).

The fidelity can be improved by stabilizing this setup. A stable source is necessary to generate photons with the same properties over a long period. As discussed earlier temperature stabilization of the compensation crystal slabs reduces phase variation of the generated photons. Moreover, slight path differences through the nonlinear crystal for the first and second pass also leads to slightly different wavelengths, which decreases the fidelity. Adjusting the focusing parameters should diminish this influence as well and increase the fidelity. If the entangled photon pair source is stabilized, then it should be possible to determine the optimal compensation crystal length more precisely and use the temperature tuning to obtain a higher fidelity.

The optimal compensation crystal length found in this work for a signal wavelength of 894.3 nm is in a good agreement with the theoretical value by using the refractive indices from Zelmon *et al.* [ZLC+10], even though they examined 0.5 % doped Nd:YVO_4. The assumption that this theoretical treatment is correct for other wavelengths must be verified for this setup by determining the optimal compensation crystal length for different wavelengths.

The current setup uses a birefringent crystal for the dispersion compensation. Using the setup for another wavelength requires removing or adding compensation crystal slabs. It would be interesting to find other materials for compensating the dispersion with an automatic tuning mechanism. Maybe AC driven birefringent liquid crystals could be used for such a task.

With this enhanced entanglement and spectral brightness the source would be ready for quantum interface applications. It is planned to transfer the information from a 894.3 nm photon emitted from a quantum dot to a 1313.1 nm photon guided into a optical fiber. This would permit a long-distance communication.

List of own publications

Articles

Otto Dietz, **Chris Müller**, Thomas Kreißl, Ulrike Herzog, Tim Kroh, Andreas Ahlrichs, Oliver Benson. *" A folded-sandwich polarization-entangled two-color photon pair source with large tuning capability for applications in hybrid quantum architectures"*, submitted (in review) to Applied Physics B

Conferences

Chris Müller, Thomas Kreißl, Tim Kroh, Otto Dietz, and Oliver Benson.
"A two-color entangled photon pair source for interfacing dissimilar quantum systems",
DPG Spring Meeting, Heidelberg (2015)

Chris Müller, Tim Kroh, Otto Dietz and Oliver Benson.
"A Two-Color Entangled Photon Pair Source for Interfacing Dissimilar Quantum Systems",
International Nano-Optoelectronics Workshop, Tokyo (2015)

References

[ASJ+13] Alan Migdall, Sergey V. Polyakov, Jingyun Fan, and Joshua C. Bienfang. *Single-Photon Generation and Detection: Physics and Applications*. Academic Press, Nov. 29, 2013.

[BB84] C.H. Bennett and G Brassard. "Quantum cryptography: Public key distribution and coin tossing". In: *Proceedings of IEEE International Conference on Computers, Systems and Signal Processing* 175 (1984). DOI: 10.1016/j.tcs.2011.08.039.

[BDC+98] H.-J. Briegel, Wolfgang Dür, Juan I. Cirac, and Peter Zoller. "Quantum repeaters: The role of imperfect local operations in quantum communication". In: *Physical Review Letters* 81.26 (1998), p. 5932. DOI: 10.1103/PhysRevLett.81.5932.

[BDE+09] Michael Bass, Casimer DeCusatis, Jay Enoch, Vasudevan Lakshminarayanan, Guifang Li, Carolyn MacDonald, Virendra Mahajan, and Eric Van Stryland. *Handbook of Optics, Third Edition Volume IV: Optical Properties of Materials, Nonlinear Optics, Quantum Optics (set): Optical Properties of Materials, Nonlinear Optics, Quantum Optics (set)*. McGraw Hill Professional, Oct. 6, 2009.

[BEZ13] Dirk Bouwmeester, Artur K. Ekert, and Anton Zeilinger. *The Physics of Quantum Information: Quantum Cryptography, Quantum Teleportation, Quantum Computation*. Springer Science & Business Media, Mar. 14, 2013.

[BGD+09] Daniel Brunner, Brain D. Gerardot, Paul A. Dalgarno, Gunter Wüst, Khaled Karrai, Nick G. Stoltz, Pierre M. Petroff, and Richard J. Warburton. "A Coherent Single-Hole Spin in a Semiconductor". In: *Science* 325.70 (2009). DOI: 10.1126/science.1173684.

[BKW13] Johannes A. Buchmann, Evangelos Karatsiolis, and Alexander Wiesmaier. *Introduction to Public Key Infrastructures*. Springer Science & Business Media, Nov. 19, 2013.

[BMD+04] B.B Blinov, D.L. Moehring, L.-M. Duan, and C. Monroe. "Observation of entanglement between a single trapped atom and a single photon". In: *Nature* 428.6979 (Mar. 11, 2004), p. 153. DOI: 10.1038/nature02377.

[Boy13] Robert W. Boyd. *Nonlinear Optics*. Academic Press, Oct. 22, 2013.

[Die15] Otto Dietz. "Secure quantum communication and light guiding: Square Gradient Bragg scattering in dielectric waveguides (Part I) and three-color folded-sandwich entangled photon source for quantum teleportation (Part II)". PhD thesis. Humboldt-Universität zu Berlin, 2015.

[DSP+10] F. Ding, R. Singh, J. D. Plumhof, T. Zander, V. Křápek, Y. H. Chen, M. Benyoucef, V. Zwiller, K. Dörr, G. Bester, A. Rastelli, and O. G. Schmidt. "Tuning the Exciton Binding Energies in Single Self-Assembled InGaAs / GaAs Quantum Dots by Piezoelectric-Induced Biaxial Stress". en. In: *Physical Review Letters* 104.6 (Feb. 2010). DOI: 10.1103/PhysRevLett.104.067405.

[FMH+80] Duan Feng, Nai-Ben Ming, Jing-Fen Hong, Yong-Shun Yang, Jin-Song Zhu, Zhen Yang, and Ye-Ning Wang. "Enhancement of second-harmonic generation in LiNbO3 crystals with periodic laminar ferroelectric domains". In: *Applied Physics Letters* 37.7 (1980), p. 607. DOI: 10.1063/1.92035.

[GFT+12] W. B. Gao, P. Fallahi, E. Togan, J. Miguel-Sanchez, and A. Imamoglu. "Observation of entanglement between a quantum dot spin and a single photon". In: *Nature* 491.7424 (Nov. 14, 2012), pp. 426–430. DOI: 10.1038/nature11573.

[GSG+08] O. Gayer, Z. Sacks, E. Galun, and A. Arie. "Temperature and wavelength dependent refractive index equations for MgO-doped congruent and stoichiometric LiNbO3". In: *Applied Physics B* 91.2 (May 2008), pp. 343–348. DOI: 10.1007/s00340-008-2998-2.

[GYS+06] A. Greilich, D.R. Yakovlev, A. Shabaev, Al. L. Efros, I.A. Yugova, R. Oulton, V. Stavarache, D. Reuter, A. Wieck, and M. Bayer. "Mode Locking of Electron Spin Coherences in Singly Charged Quantum Dots". In: *Science* 313.5785 (July 21, 2006), p. 341. DOI: 10.1126/science.1128215.

[Hec09] Eugene Hecht. *Optik*. Oldenbourg, 2009.

[HHP+09] Michael Hentschel, Hannes Hübel, Andreas Poppe, and Anton Zeilinger. "Three-color Sagnac source of polarization-entangled photon pairs". In: *Optics express* 17.25 (2009), pp. 23153–23159. DOI: 10.1364/OE.17.023153.

[JKM+01] Daniel F. V. James, Paul G. Kwiat, William J. Munro, and Andrew G. White. "Measurement of qubits". In: *Physical Review A* 64.5 (Oct. 2001). DOI: 10.1103/PhysRevA.64.052312.

[KMW+95] Paul G. Kwiat, Klaus Mattle, Harald Weinfurter, Anton Zeilinger, Alexander V. Sergienko, and Yanhua Shih. "New high-intensity source of polarization-entangled photon pairs". In: *Physical Review Letters* 75.24 (1995), p. 4337. DOI: 10.1103/PhysRevLett.75.4337.

[Kre] Thomas Kreißl. *Erzeugung von Zwei-Farben- Polarisationsverschränkung mit einem nichtlinearen Kristall in Folded Sandwich Geometrie*. Diplom Thesis, Humboldt-Universität zu Berlin (2015).

[LSP98] Hoi-Kwong Lo, Tim Spiller, and Sandu Popescu. *Introduction to Quantum Computation and Information*. World Scientific, Jan. 1, 1998.

[Mes08] Dieter Meschede. *Optik, Licht und Laser*. Springer-Verlag, Sept. 29, 2008.

[MOV96] Alfred J. Menezes, Paul C. van Oorschot, and Scott A. Vanstone. *Handbook of Applied Cryptography*. CRC Press, Oct. 16, 1996.

[MW95] Leonard Mandel and Emil Wolf. *Optical Coherence and Quantum Optics*. en. Cambridge University Press, Sept. 1995.

[NC10] Michael A. Nielsen and Isaac L. Chuang. *Quantum Computation and Quantum Information: 10th Anniversary Edition*. Cambridge University Press, Dec. 9, 2010.

[Pas08] Rüdiger Paschotta. *Encyclopedia of Laser Physics and Technology*. John Wiley & Sons, Dec. 15, 2008.

[PML+04] Matthew Pelton, Philip Marsden, Daniel Ljunggren, Maria Tengner, Anders Karlsson, Anna Fragemann, Carlota Canalias, and Fredrik Laurell. "Bright, single-spatial-mode source of frequency non-degenerate, polarization-entangled photon pairs using periodically poled KTP". In: *Optics Express* 12.15 (2004), pp. 3573–3580. DOI: 10.1364/OPEX.12.003573.

[Pow11] Peter E. Powers. *Fundamentals of Nonlinear Optics*. CRC Press, May 25, 2011.

[RSA78] Ronald L. Rivest, Adi Shamir, and Len Adleman. "A method for obtaining digital signatures and public-key cryptosystems". In: *Communications of the ACM* 21.2 (1978), pp. 120–126. DOI: 10.1145/357980.358017.

[She03] Y. R. Shen. *The principles of nonlinear optics*. Wiley-Interscience, 2003.

[SRJ+13] Fabian Steinlechner, Sven Ramelow, Marc Jofre, Marta Gilaberte, Thomas Jennewein, Juan. P. Torres, Morgan W. Mitchell, and Valerio Pruneri. "Phase-stable source of polarization-entangled photons in a linear double-pass configuration". In: *Optics Express* 21.10 (May 20, 2013), p. 11943. DOI: 10.1364/OE.21.011943.

[SSB+13] Terence E. Stuart, Joshua A. Slater, Félix Bussières, and Wolfgang Tittel. "Flexible source of nondegenerate entangled photons based on a two-crystal Sagnac interferometer". In: *Physical Review A* 88.1 (July 8, 2013). DOI: 10.1103/PhysRevA.88.012301.

[SSR+11] Nicolas Sangouard, Christoph Simon, Hugues de Riedmatten, and Nicolas Gisin. "Quantum repeaters based on atomic ensembles and linear optics". In: *Reviews of Modern Physics* 83.1 (Mar. 21, 2011), pp. 33–80. DOI: 10.1103/RevModPhys.83.33.

[ST08] Bahaa E. A. Saleh and Malvin Carl Teich. *Grundlagen der Photonik*. Wiley-VCH, 2008.

[ST14] Yoichi Sato and Takunori Taira. "Highly accurate interferometric evaluation of thermal expansion and dn/dT of optical materials". In: *Optical Materials Express* 4.5 (May 1, 2014), pp. 876–888. DOI: 10.1364/OME.4.000876.

[Ste08] Daniel Adam Steck. *Cesium D Line Data*. 2008.

[Tan96] Alice M. Tang. *Fundamentals of Optical Parametric Processes and Oscillations*. CRC Press, Mar. 1, 1996.

[TCT+10] E. Togan, Y. Chu, A. S. Trifonov, L. Jiang, J. Maze, L. Childress, M. V. G. Dutt, A. S. Sørensen, P. R. Hemmer, A. S. Zibrov, and M. D. Lukin. "Quantum entanglement between an optical photon and a solid-state spin qubit". In: *Nature* 466.7307 (Aug. 5, 2010), pp. 730–734. DOI: 10.1038/nature09256.

[TH00] Barbara M. Terhal and Paweł Horodecki. "Schmidt number for density matrices". In: *Physical Review A* 61.4 (2000), p. 040301. DOI: 10.1103/PhysRevA.61.040301.

[TW08] Pavel Trojek and Harald Weinfurter. "Collinear source of polarization-entangled photon pairs at nondegenerate wavelengths". In: *Applied Physics Letters* 92.21 (2008), p. 211103. DOI: 10.1063/1.2924280.

[VWS+06] Jürgen Volz, Markus Weber, Daniel Schlenk, Wenjamin Rosenfeld, Johannes Vrana, Karen Saucke, Christian Kurtsiefer, and Harald Weinfurter. "Observation of Entanglement of a Single Photon with a Trapped Atom". In: *Physical Review Letters* 96.3 (Jan. 25, 2006). DOI: 10.1103/PhysRevLett.96.030404.

[Wei] Oliver Weisse. *Quantum Eraser für Quantenkommunikationsanwendungen*. Bachelor Thesis, Humboldt-Universität zu Berlin (2015).

[WGP+07] Andrew G. White, Alexei Gilchrist, Geoffrey J. Pryde, Jeremy L. O'Brien, Michael J. Bremner, and Nathan K. Langford. "Measuring two-qubit gates". In: *JOSA B* 24.2 (2007), pp. 172–183. DOI: 10.1364/JOSAB.24.000172.

[WSB+04] A. Wallraff, D. I. Schuster, A. Blais, L. Frunzio, R.-S. Huang, J. Majer, S. Kumar, S.M. Girvin, and R.J. Schoelkopf. "Strong coupling of a single photon to a superconducting qubit using circuit quantum electrodynamics". In: *Nature* 431.7005 (Sept. 9, 2004), p. 162. DOI: 10.1038/nature02851.

[WZ82] W. K. Wootters and W. H. Zurek. "A single quantum cannot be cloned". In: *Nature* 299.5886 (Oct. 28, 1982), pp. 802–803. DOI: 10.1038/299802a0.

[YNS+93] M. Yamada, N. Nada, M. Saitoh, and K. Watanabe. "First-order quasi-phase matched LiNbO3 waveguide periodically poled by applying an external field for efficient blue second-harmonic generation". In: *Applied Physics Letters* 62.5 (1993), p. 435. DOI: 10.1063/1.108925.

[ZLC+10] David E. Zelmon, Julie J. Lee, Kelly M. Currin, Jessica M. Northridge, and Dan Perlov. "Revisiting the optical properties of Nd doped yttrium orthovanadate". In: *Applied optics* 49.4 (2010), pp. 644–647. DOI: 10.1364/AO.49.000644.

[Foc15] Foctek Photonics, Inc. *YVO4*. 2015.

A Sellmeier equations

The Sellmeier equation gives the refractive index of a material for different wavelengths. This empirical relationship is determined by measuring the refractive index for several wavelengths. A fit gives the refractive index for other wavelengths. This kind of determination leads to different results depending on the setup, measured wavelength, theoretical model and purity of the material. Note that the wavelength has to be in microns because of the units of the coefficients.

A.1 Yttrium orthovanadate

YVO_4 crystals are used in this work to compensate the dispersion from the generation scheme. Unfortunately, the Sellmeier equation of YVO_4 varies in the literature. The Equations A.1-A.4 show the different Sellmeier equation for different references and the Tables A.1-A.4 give the corresponding coefficients of these Sellmeier equations.

Foctek Photonics, Inc. [Foc15]

$$n^2(\lambda) = A + \frac{B}{\lambda^2 - C} - D\lambda^2 \tag{A.1}$$

Table 5: Sellmeier equation coefficients for YVO_4 from Foctek Photonics, Inc. [Foc15].

parameters	ordinary axis	extraordinary axis
A	3.77834	4.5909
B	0.069736	0.110534
C	0.04724	0.04813
D	0.0108133	0.0122676

Zelmon *et al.* [ZLC+10]

$$n^2(\lambda) = A + \frac{B}{\lambda^2 - C} + \frac{D\lambda^2}{\lambda^2 - E} \tag{A.2}$$

Table 6: Sellmeier equation coefficients for 0.5 % Nd:YVO_4 from Zelmon *et al.* [ZLC+10].

parameters	ordinary axis	extraordinary axis
A	2.3409	2.7582
B	1.4402	1.853
C	0.04825	0.056986
D	1.8698	3.0749
E	171.27	195.06

Sato *et al.* [ST14]

$$n^2(\lambda) = A + \frac{B}{\lambda^2 - C} - D\lambda^2 \tag{A.3}$$

Table 7: Sellmeier equation coefficients for YVO_4 from Sato *et al.* [ST14].

parameters	ordinary axis	extraordinary axis
A	3.79300	4.63100
B	0.06437	0.09736
C	0.05641	0.06466
D	0.01428	0.02189

Handbook of Optics [BDE+09]

$$n^2(\lambda) = A + \frac{B}{\lambda^2 - C} - D\lambda^2 \tag{A.4}$$

Table 8: Sellmeier equation coefficients for YVO_4 from Handbook of Optics [BDE+09].

parameters	ordinary axis	extraordinary axis
A	3.778790	4.607200
B	0.074790	0.108087
C	0.045731	0.052495
D	0.009701	0.014305

A.2 Lithium niobate doped with 5% magnesium oxide

Gayer *et al.* measured the wavelength and temperature dependent refractive index of lithium niobate doped with 5 % magnesium oxide [GSG+08]. It is assumed that the Sellmeier equation has the form

$$n^2(\lambda) = a_1 + b_1 f + \frac{a_2 + b_2 f}{\lambda^2 - (a_3 + b_3 f)^2} + \frac{a_4 + b_4 f}{\lambda^2 - a_5^2} - a_6 \lambda^2 \tag{A.5}$$

where the parameter a_1 gives the contribution from plasmons in the far infrared, a_2 and a_5 calculates the poles in the ultraviolet and infrared wavelengths, with a_2 and a_4 as weighting factors. The thermal effects are described by the b_i coefficient, involving the parameter f

$$f = (T - 24.5\,^\circ)(T + 570.82\,), \tag{A.6}$$

which gives the temperature dependence.

The refractive index of the Sellmeier equation from Equation (A.5) can be written as

$$n(\lambda) = \sqrt{a_1 + b_1 f + \frac{a_2 + b_2 f}{\lambda^2 - (a_3 + b_3 f)^2} + \frac{a_4 + b_4 f}{\lambda^2 - a_5^2} - a_6 \lambda^2}. \tag{A.7}$$

For calculating the bandwidth of a photon (see Section 2.1.3) the partial derivative of the wavelength λ is necessary

$$\frac{\partial n}{\partial \lambda} = \frac{1}{2n} \left(-\frac{(a_2 + b_2 f) 2\lambda}{(\lambda^2 - (a_3 + b_3 f)^2)^2} - \frac{(a_4 + b_4 f) 2\lambda}{(\lambda^2 - a_5^2)^2} - 2 a_6 \lambda \right). \tag{A.8}$$

Note that the derivative $\frac{\partial n}{\partial \lambda}$ is not dimensionless but has the unit $1/\mu m$.

Table 9: Sellmeier equation coefficients for lithium niobate doped with 5 % magnesium oxide from Gayer *et al.* [GSG+08].

parameters	ordinary axis	extraordinary axis
a_1	5.653	5.756
a_2	0.1185	0.0983
a_3	0.2091	0.2020
a_4	89.61	189.32
a_5	10.85	12.52
a_6	$1.97{\cdot}10^{-2}$	$1.32{\cdot}10^{-2}$
b_1	$7.941{\cdot}10^{-7}$	$2.860{\cdot}10^{-6}$
b_2	$3.134{\cdot}10^{-8}$	$4.700{\cdot}10^{-8}$
b_3	$-4.641{\cdot}10^{-9}$	$6.113{\cdot}10^{-8}$
b_4	$-2.188{\cdot}10^{-6}$	$1.516{\cdot}10^{-4}$

A.3 BK7

BK7 is a glass commonly used to fabricate optical components, including the Fresnel rhomb from this setup. Equation A.9 gives the Sellmeier equation for BK7 and Table 10 contains the corresponding coefficients.

$$n(\lambda)^2 = 1 + \frac{B_1\lambda^2}{\lambda^2 - C_1} + \frac{B_2\lambda^2}{\lambda^2 - C_2} + \frac{B_3\lambda^2}{\lambda^2 - C_3} \tag{A.9}$$

Table 10: Sellmeier equation coefficients for BK7 [Mes08].

parameters	
B_1	1.0396
B_2	0.23179
B_3	1.0105
C_1	0.0060
C_2	0.200
C_3	103.56

Acknowledgments

First I want to thank Prof. Dr. Oliver Benson for the opportunity to work in the Nano-Optics group and for supervising this work.

Furthermore, I want to acknowledge Otto Dietz for his support. His guidance was always very helpful and I learned a lot from him. It was always pleasant to discuss problems with him. I am very grateful to him. Thank you.

I want to thank Tim Kroh for his help over the course of many hours. He taught me many new things in and outside of the lab. He always had time if I needed advice or some other help.

I would like to thank Andreas Ahlrichs for his interest in this work. I changed my plans often after I talked to him since he shared his experience and showed better ways to deal with several problems.

Thomas Kreißl began the geometrical folded sandwich and introduced it to me, allowing us to finish it finished together. He taught me a lot and he was very reliable. It was a pleasure to work with him. Thanks.

Additionally, I want to thank the entire Nano-Optics group and the Optical Meteorology group for the very wonderful working atmosphere. I really like that both groups are working quite closely and help each other.

The study was quite long and very work-intensive. I would not behave been able to complete my bachelor or master degree without the help of my fellow students Max, Hans, Pascal, Alex and Sven. It was very exhausting to work on several tasks, but it was nice to work with them. Thank you!

I am thankful that I met Katherine during my master. She helped and still helps me to improve my English. With that help it was much easier to write this thesis. She explained a lot to me and I am curious how much she will teach me in the future.

I thank all my other friends as well that they showed me that there is a life outside of the university. There were times when I almost forgot that.

Last but not least, I would like to thank my family. Studying without their support would be much more difficult or maybe even impossible for me. My parents supported me not only financially, they also helped me in many other things so that I could concentrate on my studies. My brother encouraged me quite often in his special way and helped with many formal issues.

Eigenständigkeitserklärung

Hiermit versichere ich, dass ich die vorliegende Arbeit selbständig verfasst und keine anderen als die angegebenen Quellen und Hilfsmittel verwendet habe.

Ort, Datum	Unterschrift